

See discussions, stats, and author profiles for this publication at: <https://www.researchgate.net/publication/231650791>

Structures of Zinc Oxide Nanoclusters: As Found by Revolutionary Algorithm Techniques

ARTICLE *in* THE JOURNAL OF PHYSICAL CHEMISTRY C · NOVEMBER 2008

Impact Factor: 4.77 · DOI: 10.1021/jp805983g

CITATIONS

58

READS

86

4 AUTHORS, INCLUDING:



[Abdullah A. Al-Sunaidi](#)

King Fahd University of Petroleum and Min...

18 PUBLICATIONS 274 CITATIONS

[SEE PROFILE](#)



[Richard Richard A Catlow](#)

University College London

998 PUBLICATIONS 24,830 CITATIONS

[SEE PROFILE](#)



[Scott M Woodley](#)

University College London

80 PUBLICATIONS 1,915 CITATIONS

[SEE PROFILE](#)

Structures of Zinc Oxide Nanoclusters: As Found by Revolutionary Algorithm Techniques

Abdullah A. Al-Sunaidi,[†] Alexey A. Sokol,[‡] C. Richard A. Catlow,[‡] and Scott M. Woodley^{*,‡}

Physics Department, King Fahd University of Petroleum and Minerals, Dhahran 31261, Saudi Arabia, and Department of Chemistry, University College London, Third Floor, Kathleen Lonsdale Building, Gower Street, London WC1E 6BT, United Kingdom

Received: July 7, 2008; Revised Manuscript Received: August 22, 2008

We report the stable and low energy metastable structures of zinc oxide clusters, $(\text{ZnO})_n$, $n = 1–32$, found using an evolutionary algorithm with polarizable shell interatomic potentials. This study comprises the first systematic search for nanoparticulate structures for this compound above $n = 18$ and includes a comparison with other recent studies. As a function of n , global minimum and low energy metastable clusters evolve from rings (up to ca. 0.8 nm in diameter) to perfect closed bubbles (up to ca. 1.2 nm in diameter in the range reported), which are the structures that only contain tetragonal and hexagonal faces and all ions have a coordination number of three. The transition between the two structural families is blurred, with key structures that are also (i) open bubbles, which contain octagonal or larger faces, and (ii) bubbles that have handles, or two-dimensional ring fragments attached. A new nomenclature to describe these structures is defined. We find a greater stability of tetrahedral and trigonal coordinations compared to tetragonal for ZnO clusters in the range considered. Of the predicted global minimum clusters, spheroid cages $n = 12$, 16, and 28, with symmetry point groups T_h , T_d and T , and barrels, which are a common motif, exhibit a relatively high stability. Bulklike wurtzite, or multilayered clusters, as well as the simple cuboid and related rock salt configurations are not found to be thermodynamically stable in the size range considered.

Introduction

In recent years, there has been growing interest in studying the properties of metal oxide nanostructures. In particular, considerable attention has been given to zinc oxide as a promising multifunctional material with wide-ranging technological applications including electrical and light-emitting devices, gas sensors, and catalysis.^{1,2} As a semiconductor with a band gap of 3.37 eV (at room temperature) and a large exciton binding energy of 60 meV, ZnO has been recognized as a valuable optical material in the blue-UV region.³

Low-dimensional structures of ZnO have been synthesized as ultrathin films or nanosheets, nanorods, and nanotubes, with various morphologies reported: whiskers, belts, flowers, pyramids, as well as nanoparticles, which are observed in a gas phase, as liquid colloids, and stabilized on surfaces or encapsulated in solid-state materials. Moreover, nanocomposite materials, where individual nanoparticles make building blocks, have also been synthesized in varying shapes and architectures. In this work, we focus on the atomic structure of ZnO nanoparticles, which may apply to many other binary systems with 1:1 stoichiometry.

In differing applications of ZnO, structural and optical properties are crucially determined by the size of particles. Three regimes, or length scales, are recognized (cf. work on ZnO by Wood et al.⁴):

(1) Macroscopic: Particles maintain the crystal structure of the bulk; the optical band gap is practically constant, while point defects and surfaces give rise to specific size-independent phenomena, e.g., UV, blue-green, yellow-orange, and red luminescence;

(2) Quantum dots: At least in one dimension, the particle size is of the order of the exciton radius, 15–30 Å. In this regime, the bulk crystal structure is preserved even though the X-ray diffraction lines broaden, while the order of stability between the phases could change, whereas the optical absorption bands shift and deform, owing to quantum-size effects.

(3) Clusters: The structure of the particles may significantly differ from that of the bulk phases. Moreover, no clear diffraction patterns are obtainable, and optical properties cannot be directly correlated with those of the bulk. For ZnO, in contrast to other materials, there has not yet appeared an experimental technique capable of reliable characterization of the local structure; this regime is understood least.

No clear transition on the size scale has been found between the quantum dot and cluster regimes in ZnO (or in other materials). And the problem of accurate experimental structure determination for small particles with sizes below 5–10 nm, where standard X-ray diffraction techniques start to fail, has not been resolved satisfactorily. By use of novel refinement techniques,⁵ some progress has recently been achieved for the low nanometer particles, which preserve the bulk crystal structure even when the concentration of defects is high. In other cases, which are of particular interest here, the current approaches either rely on direct observation by microscopic methods, which are very difficult and provide information only about approximate shape and size of the particles, or on optical UV/vis absorption spectroscopy, which exploits quantum-size effects. The latter approach, however, is questionable as the true correlation between the absorption edge and the particle size is based on oversimplistic quantum confinement hypotheses,⁶ with no regard for the changes with size in the local structure and particle surface effects (cf. ref 7 where particles are assumed to be spherical and an effective mass model is used).⁷ In fact, no reliable parametrization of the quantum size formulas has

* To whom correspondence should be addressed. E-mail: Scott.Woodley@ucl.ac.uk.

[†] King Fahd University of Petroleum and Minerals.

[‡] University College London.

been established for ZnO. Wood et al.⁴ have separated a semiconductor quantum dot and cluster regimes in the nucleation and growth of ZnO particles (1–6 nm in size), with the latter taking place above ca. 1 nm size, and found that the observed optical spectra do not satisfy the usual simple quantum-size models. Hence, computational methods, aimed at structure prediction in the sub- and low-nanometer range of particles sizes, are crucial for further progress in this area.

There have been a number of previous computational studies of the structure of small ZnO nanoparticles. Before discussing this literature, we give a brief review of experimental evidence relating to their preparation and characterization.

The many proposed optical applications of ZnO nanoparticles would rely on the availability of monodispersed quantum dots or clusters with tunable optical properties, which would depend on particle shape and size and a high quantum yield. On the other hand, maintaining the high surface area of nanoparticulate material is important for catalytic applications, with relatively broad size distributions being acceptable. Capping of nanoparticles by various passivating species as well as encapsulation in chemically unreactive environments (typically using amorphous media) prevents further growth and coagulation of the particles and has allowed a better uniformity in size to be attainable.^{8–10} Unfortunately, there is also a significant loss of quantum yield in emission spectra and catalytic activity.¹¹ Surface or interface effects can change dramatically both the intensity and the position of absorption and emission bands,¹² as has been highlighted, for example, by Zhou et al.¹³ when investigating ZnO quantum dots (with the sizes of 4.8, 5.3, and 7.0 nm) under wet conditions, resulting in coverage by a thin shell of zinc hydroxide.

Although various ZnO nanostructures have been synthesized and characterized, preparing small ZnO nanoparticles is known to be a difficult process since clusters tend to aggregate very quickly forming large nanoparticles. Broad size distributions including sub- and low-nanometer particles have been reported by applications of various techniques. In one example, Vostrikov et al.^{14,15} characterized the kinetics of synthesis reactions of solid and liquid Zn with supercritical water to produce $(\text{ZnO})_n$ and H_2 and observed a size distribution from 1.5 to 150 nm, with a mean value of 60 nm. They argued that the reactions become highly exothermic after a critical cluster size, which was estimated to be around $n = 7$, and that smaller clusters are probably generated by a collective reaction of a number of Zn atoms with water. These smaller clusters were found on the surface of solid Zn, where the clusters grow by a monomeric stepwise process (epitaxy), or to be a highly mobile species in liquid Zn resulting in the small clusters coagulating.

Better control over the particle size distribution was achieved by a gas-phase approach using the heterocubane $(\text{ZnO})_4$ compound, $[\text{CH}_3\text{ZnOCH}(\text{CH}_3)_2]_4$, by Polarz et al.,¹⁶ who were able to obtain a narrow size distribution, even though the smallest reported particles were of ca. 3 nm in diameter. These authors also observed fast coagulation and sintering of ZnO particles. Smaller size particles (down to 1.3 nm) with a narrow distribution (10%) were obtained by Hartlieb et al.¹⁷ under continuous flow using spin disk processing, from zinc nitrate hexahydrate.

By use of time-of-flight mass spectroscopy, small ZnO clusters of particular mass have been identified in plasma plumes obtained by laser ablation of Zn and ZnO targets in various atmospheres. Neutral molecular clusters in the gas phase are particularly difficult to observe, and a monomeric $(\text{ZnO})_1$ species has only recently been found in a molecular beam.¹⁸ In the first

report by Burnin and BelBruno,¹⁹ positively charged $(\text{ZnO})_n$ clusters in the range of $n = 5–20$ were observed. Moreover, a relatively smooth ZnO particle distribution was contrasted with that of ZnS, which exhibits a pronounced peak at $n = 13$ (the so-called magic number). Bulgakov et al.²⁰ reported both stoichiometric and nonstoichiometric Zn_nO_m particles with n up to 16; curiously, these authors observed magic number clusters at $n = 9, 11$, and 15 and a local abundance minimum at $n = 13$. Kukreja et al.²¹ have recorded fully resolved mass spectra for $(\text{ZnO})_n$ up to $n = 20$, both positively and negatively charged, and in addition, nonstoichiometric clusters with an excess of either Zn or O. Most recently, there has appeared a report by Dmytryk et al.²² who mentioned the appearance of magic number clusters for ZnO clusters of larger size, with the cluster range of $20 < n < 200$ explored, but no details were given.

ZnO clusters prepared by laser ablation have been deposited on substrates²³ or collected in gas-suspended nanoaggregates,^{24,25} where they typically coalesce to 10–20-nm size particles with a relatively broad size distribution. Still smaller nanoparticles (of the order of 1 nm) have been obtained by laser ablation in liquid media, e.g., deionized water and ethanol, as confirmed by microscopic techniques.²⁶ Synthesis of ZnO clusters in plasma plumes and the dynamics of their growth have been inferred from their luminescence spectra.²⁷ ZnO nanoclusters were also synthesized by sputtering a Zn target with Ar^+ ions in an atmosphere of Ar, He, and O_2 gases.²⁸ The Zn atoms coalesce with oxygen and argon atoms due to three-body collisions to form ZnO nanoclusters. The particles formed are much larger than the clusters identified in ablation plumes, with an average size of 7 nm, and the structure of these particles is that of the bulk, hexagonal wurtzite ZnO.

In early attempts to control the cluster size and morphology, encapsulated ZnO clusters were prepared within the pores of microporous materials, e.g., siliceous and Al-containing zeolites.^{29,30} However, because of the high degree of disorder and inherent difficulties in characterization of Zn, the structures of the encapsulated particles have remained largely unresolved³¹ (cf. 1–2-nm particles size, deduced in ref 31), while relevant optical properties were reported.^{32,33} Moreover, the strong interaction between the charged silicate framework and the extraframework cluster is expected to result in a strongly cationic nature of the clusters. For example, only three to four oxygen atoms were found to coordinate a body-centered cubic Zn cluster ($\text{Zn}_9\text{O}_{3–4}$) inside a sodalite cage of zeolite LTA.³⁴ ZnO particles were also encapsulated by various techniques in optically transparent media including silica glass and mesoporous siliceous materials.³⁵

Finally, we highlight the work of Wu et al.,³⁶ who have prepared small $(\text{ZnO})_n$, $n = 1–15$, nanoclusters (with size 3–10 Å) using the electroporation of unilamellar vesicles. The growth of the clusters was associated with novel alternating, red and blue, shifts of the absorption edge. They compared their data with theoretical predictions from density functional theory (DFT) for the structure and time-dependent (TD) DFT for the optical-transition-based calculations³⁷ and matched the maxima and minima in the absorption bands at $n = 2, 5, 12$ for the range 1–16.

Computer simulations have made a major contribution to the understanding of the structure and stability of different metal oxide nanoclusters. Clusters are assumed to adopt the configuration with the lowest energy of formation. As n increases, the complexity of the energy landscape explodes, and the enumeration of the possible structures quickly becomes intractable. In this paper, we seek, in the first instance, the structures

on these landscapes with the lowest energy of formation, i.e., the global minima (GM). However, the level at which the energy is calculated may prove to be insufficiently accurate, or other, higher-energy configurations could be realized in nature as determined by thermodynamic or kinetic conditions. Therefore, we choose to target not just the GM but also a number of key, low-energy metastable structures. We have applied three approaches to the problem of searching over the configurational space: (i) relaxation of structural fragments cut from the known bulk phases of ZnO, (ii) relaxation of structures built by construction, or rational design, from small units (typically, ground-state structures for small n), and (iii) the application of an evolutionary algorithm (EA). However, to place our study into context we now summarize the previous computational work applied to the structure prediction of ZnO clusters.

In a pioneering study on the stability of small ZnO clusters, Behrman et al.³⁸ performed several molecular dynamics simulations, where the interactions were described using Coulomb along with Buckingham short-range interatomic potentials. Their simulations, supported by quantum-mechanical (semiempirical, PM3, and ab initio, Hartree–Fock using a minimum basis set) calculations, suggested that, for certain clusters, $(\text{ZnO})_n$, $n = 4, 6, 11, 12$, and 15 , the ground state takes the form of a cube, hexagonal prism, and hollow spheroids. Although these studies found the hollow spheroids with $n < 11$ not to be absolutely stable, they suggested, by comparison with carbon fullerenes, that $n = 12$ and 16 are possible magic numbers, and performed the first DFT calculations, with a larger basis set, to confirm the stability of these clusters.³⁹

The first systematic study of small ZnO clusters ($n = 1–9$), using DFT techniques (a hybrid, B3LYP, exchange and correlation functional and a Gaussian-type basis set), was reported by Matxain et al.⁴⁰ The GM were predicted to be rings for $n = 2–7$, an octagonal prism for $n = 8$, and a hollow spheroid for $n = 9$. Their work was expanded³⁷ to include hollow spheroids up to $n = 15$ and predicted the lowest excitation energies (calculated with TD DFT), which for ringlike structures ($n < 8$) are larger than those of the spheroid structures ($n \geq 8$).

A number of other studies using DFT techniques have been reported more recently. For example, Jain et al.⁴¹ have studied the stability of clusters with $n < 7$, using DFT (with a generalized gradient approximation, GGA, exchange and correlation functional, ultrasoft pseudopotentials and a plane-wave basis set), and also found for $n > 1$ the ring structures to be the GM. Reber et al.^{42,43} reported the GM structures and electronic properties for $n = 2–18$ and 21 , calculated using the GGA with a Gaussian basis set (it remains unclear though how “a total of 200 initial geometric configurations” were generated), with $n = 10, 13$, and 14 GM clusters differing from those reported in ref 33. Zhao et al.⁴⁴ constructed bubblelike clusters from tetragonal and hexagonal rings for $n = 9–16, 18, 20, 22, 24, 28, 36, 48$, and 64 and compared their stability with the smallest, $n = 16, 20, 26, 32$, and 44 , solid prismatic clusters cut from the wurtzite crystal structure. In addition, one onionlike (double-wall bubble) structure, $n = 60$, has been built by insertion of an $n = 12$ cage inside of an $n = 48$ cage, which was found to be 0.2 eV/atom more stable than the corresponding single-wall bubble. Interestingly, these authors predicted $n = 26$ to be the point of transition between bubble and wurtzite structured clusters.

Li et al.⁴⁵ have concentrated on properties of perfect hexagonal prism structures for $n = 6, 12, 24$, and 48 and observed spontaneous structural transformation from wurtzite

to rock salt for $n = 24$ (using GGA and a numerical atomic basis set). Zhu et al.⁴⁶ also used GGA and a numerical basis set, but complemented these calculations with tight binding investigations to optimize geometries of predefined bubble (fullerene)-like clusters for $n = 12, 16, 28, 36, 48$, and 76 . Larger-sized clusters, up to ca. $n = 80$, initially spherical and cubic cuts from bulk wurtzite and zinc blend, have been studied by Joswig et al.⁴⁷ using a parametrized tight-binding DFT. These authors found that after relaxation the general shape of the clusters was preserved, with the surface relaxation effects confined within a surface layer, $2.5–3$ Å thick, Zn ions relaxed inward and O ions outward.

The next systematic search of the GM structures for $n = 1–18$ was reported by Wang et al.,⁴⁸ who applied a genetic algorithm approach to generate the clusters, which were optimized using the GGA level of theory along with a numerical atomic basis set. These authors reported the crossover from ring to hollow structures at $n = 8$ and, more importantly, identified two families of the hollow structures, cage- and tubelike, that compete in this range to be the GM. Larger size structures were later constructed by these authors, using experience gained and chemical intuition rather than the genetic algorithm, for $n = 24, 28, 36$, and 48 , and they concluded that cage and tube structures were still preferred.⁴⁹

The structures of ZnO clusters encapsulated in zeolites have also been investigated (see ref 50 and references therein for comparison). Lim et al.⁵⁰ used the method of interatomic potentials and energy minimization techniques applied to the most stable configurations produced within a grand canonical Monte Carlo simulation. The $n = 1–7$ clusters have been found to fit within a β (or sodalite) cage of zeolite Y, with some lower-energy configurations only metastable in the gas phase.

In this paper, we report on our quest for the most stable structures for $(\text{ZnO})_n$ clusters of size $n = 1–32$ using only the EA approach; our results from the other approaches, listed as (i) and (ii) above, will be reported elsewhere. We are interested in determining the range of cluster size that certain structural motifs are particularly stable; once known, such structural motifs may be more easily constructed. Simultaneously, our confidence in whether the EA is successful at finding the desired structures is tested, as the constructed structures should either be part of the set originally found or higher in energy. EAs, which include the more familiar genetic algorithms as a subclass, are very powerful in searching for GM of clusters.⁵¹ Although the GM clusters above $n = 100$ have been successfully located for Lennard-Jones systems, for real ionic materials only smaller size clusters have been reported so far, owing to the dramatically increased complexity of the configurational space, which could partly be related to the long-range character of the Coulomb interactions. Recent examples include $(\text{MgO})_{n=1–35}$,⁵² $(\text{SiO}_2)_{n=1–12}$,⁵³ $(\text{TiO}_2)_{n=1–15}$.⁵⁴ Interatomic potentials are typically fitted to the observed structure and various properties of the bulk phase, and there is always a debate as to whether such potentials are valid for modeling small-sized clusters, which necessitates the corroboration of the geometries of the more stable clusters using, for example, DFT. The interatomic potentials used here were originally derived for modeling the structure of bulk ZnO and its surfaces. As the majority of atoms within small clusters are associated with a surface, we expect that this potential will be adequate. In a subsequent publication, we will report how the stable and metastable structures found here behave on energy minimization with DFT calculations. We can confirm that the change in the structural parameters for the more stable

configurations of several clusters in the range of $n = 1\text{--}28$ is within 0.05 Å and that the mean energy change is within 0.1 eV/ZnO, which is comparable to that we found on varying basis sets and exchange correlation functionals.

Previously proposed structures for ZnO clusters can be categorized into families: sticks, rings, tubes, rods, spheroids (sometimes referred to as bubbles), multilayered spheroids (onions), bulklike, and others. Particular motifs are easier to explore systematically, and this approach has been applied to the investigation of ZnO structures, which has stimulated much experimental work on small clusters.

Computational Methodology

To determine the most stable structures, an EA is employed, which generates candidate, or trial, configurations while simultaneously filtering out implausible and other unwanted configurations.⁵⁴ The fundamental idea behind the EA is to perform a process that mimics natural selection through survival of the fittest. The end product of each EA cycle is a new population of candidate structures. Over several iterations, the quality of the candidates improves so that one of the candidates generated is the desired “best-fit” structure: in our case, the ground-state configuration for a cluster with a predefined composition. In the first EA cycle the candidate structures are configurations in which the ionic coordinates are randomized. During each cycle, tournaments between pairs of candidate structures, randomly selected from the current population, are simulated so that the winning candidates become parents, i.e., go on to breed new candidate structures. Probabilities are set so that candidates with the lower cost function (energy) are more likely to form children structures that resemble both their parents but may also have a few unique features (due to mutations). Breeding, or the creation of new configurations, is achieved by concatenating information (e.g., ionic coordinates) taken from the parents, and mutations are achieved by making random displacements of one or two ions. In this study, our EA makes use of the local optimization routines within the GULP program to relax all newly created structures (whether through breeding or randomization). Finally, on the last EA cycle, the better clusters within the final population, as measured by the energy of formation, are selected for analyses or further refinement. To characterize the performance of the EA search for more stable structures, we report the success rate from a subset of calculations: for each n we run the EA ten times with 1,000 cycles and a population size of 20 candidates, where all twenty candidates in the final population for all ten runs form the statistical ensemble. In these calculations: (a) in each cycle, ten candidate structures, chosen by natural selection from the current (soon to be discarded) population, form part of the new population; (b) the clusters are confined within a container of 16 Å diameter (assuming we do not want fragmented clusters, to increase efficiency of the EA, the maximum distance between ions of a cluster is constrained); and (c) within the evolving population, candidate structures with an energy difference of less than 0.01 eV are eliminated and replaced by a random structure (our crude measure of identical structures, which need to be eliminated to help keep structural diversity of the population high in order to increase the efficiency of the EA). We have also carried out further runs using, for example, different size containers and numbers of EA cycles, which allowed us to tune and place additional checks on the procedure chosen. However, we note that the corresponding results have not been included in the final statistical analysis.^{54,55}

During the EA search, many configurations need to be considered and, therefore, it would be too expensive and in many

cases irrational to use an ab initio (e.g., DFT) approach when initially measuring the suitability of each. Furthermore, different currently available ab initio methods can predict different GM structures for the same system,⁵⁶ and therefore, results still need to be calibrated against experiment. A robust and computationally inexpensive method of interatomic potentials has been employed instead. During the EA search, as a first estimate we have used a rigid ion model (RM), where the cost function is the energy of formation, E_f , expressed as a sum of pairwise interatomic potentials between rigid ions, represented by point charges. E_f is calculated with respect to isolated constituent ions, in contrast with ab initio calculations where the binding energies are defined with respect to neutral atoms and where a constant term should be added for comparison with our results. After our search, when the better candidate structures are refined, the Shell Model (SM) is employed, which takes into account electronic polarization effects. Our chosen interatomic potentials consist of a Coulomb part

$$U_{ij}^{\text{Coul}} = k \frac{q_i q_j}{r_{ij}} \quad (1)$$

where q_i is the point charge representing the ion (or its core or shell, when using the SM), k a dimensional constant, and r_{ij} the distance between two point charges, i and j , and of a short-range part, the form of which is dependent on the value of r_{ij} and is composed of three different potential functions: (i) a Buckingham potential

$$U_{ij}^{\text{Buck}} = A_{ij} \exp\left(-\frac{r_{ij}}{\rho_{ij}}\right) - \left(\frac{C_{ij}}{r_{ij}^6}\right) \quad (2)$$

(ii) a Lennard-Jones potential

$$U_{ij}^{\text{LJ}} = \frac{B_{ij}}{r_{ij}^{12}} - \frac{D_{ij}}{r_{ij}^6} \quad (3)$$

and (iii) a polynomial potential

$$U_{ij}^{\text{polyn}} = a_{ij} + b_{ij} r_{ij} + c_{ij} r_{ij}^2 + d_{ij} r_{ij}^3 + e_{ij} r_{ij}^4 + f_{ij} r_{ij}^5 \quad (4)$$

The species dependent potential parameters, A , B , C , D , ρ , a , b , c , d , e , and f , are given in Table 1.⁵⁷

The chosen interatomic potential parameters were previously derived within the SM to investigate surface and bulk properties of zinc oxide.⁵⁸ In particular, we note that the constants in eq 4 were defined so that the resultant interatomic potential is smooth and continuous between the regions where eqs 2 and 3 are employed. During the EA search, when the RM model is employed, formal charges on the zinc ($q = +2$) and oxygen ($q = -2$) ions are used, and as noted, polarization effects were, during the final refinement, reintroduced into our model by using the SM. All calculations were performed using the GULP software package.^{54,59,60}

Finally, we note that, in our analyses and visualization, coordinations of O to Zn, coordination of Zn to O, and Zn–O bond formation is defined using a maximum interatomic Zn–O distance of 2.4 Å.

Results and Discussion

The EA, as described above, generates a population of candidates, each a stationary point on the energy landscape, which evolves toward lower-energy solutions. During each search, for a specified value of n , we find several different structures (isomers). The “better” candidate isomers, as measured by the energy of formation, E_f , are, for convenience,

TABLE 1: Potential Parameters Used for This Study^a

Buckingham potentials (eq 2)	range (Å)	A (eV)	ρ (Å)	C (eV Å ⁶)
Zn (core) - O (shell)	0.0–2.2	592.342818	0.352159	12.896893
Zn (core) - O (shell)	3.1–3.3	157.297013	0.429673	5.815914
Zn (core) - O (shell)	3.6–12.0	912.517869	0.078935	11.723055
O (shell) - O (shell)	0.0–12.0	23674.698081	0.226404	33.476469
Lennard-Jones (eq 3)	range (Å)	B (eV Å ¹²)	D (eV Å ⁶)	
Zn (core) - O (shell)	0.0–2.2	316.435204	0.000000	
Zn (core) - Zn (core)	0.0–12.0	20000.0000	30.000000	
polynomial potentials (eq 44)	range (Å)	a (eV)	b (eV/Å)	c (eV/Å ²)
Zn (core) - O (shell)	2.2–3.1	111.901725	-158.72704	89.657363
Zn (core) - O (shell)	3.3–3.6	64102.354057	-93216.170229	54188.807
		d (eV/Å ³)	e (eV/Å ⁴)	f (eV/Å ⁵)
		-24.98635	3.399631	-0.177932
		-15741.070904	2284.873362	-132.581025

^a Point charges of Zn core, O core, and O shell are 2.0, 1.754415, and -3.754415 eel, and the spring constants between O core and O shell are 55.518883 eV/Å² and 2625.567362 eV/Å⁴.

labeled as *na*, *nb*, *nc*,... etc., where “a” refers to the isomer of size *n* that is found with the lowest energy of formation, our GM structure for size *n*, “b” the next-lowest energy configuration, a metastable isomer, “c” the third-lowest energy isomer, etc. Lower case letters signify that the RM is used, whereas upper case letters refer to SM calculations. In a few exceptional cases we have also included, in this list, clusters where E_f corresponds to a saddle point on the potential energy landscape; these structures are indicated by the use of an asterisk. As the order of stability for different configurations for a cluster containing the same constituent ions may change depending on the chosen model, we report, in each case, the set of lowest energy structures found for each size of cluster.

Before reporting our results, we can anticipate that the structures will be characterized by certain features: their dimensionality, ion coordination, and connectivity, which are all interlinked, and larger clusters may also be considered as a collection of smaller clusters or structural units. From our experience and from previous studies, as clusters grow, the dimensionality and ion coordination will increase from linear chains of one/two-coordinated ions to polygons (*m*-member rings). Then, the polygonal structural units, in turn, can be aligned in a patchwork or a stack to create either a two or a three-dimensional body. Alternatively, the polygons can be merged, creating edge-sharing regions, to form either 2D patchworks or 3D networks. Furthermore, the 2D patchworks can bend in the third dimension to create tubes with ends that are either left open or capped and spheroids or other open structures, see below. Finally, three-dimensional structural units can also be stacked or merged, by face sharing, to create a patchwork of polyhedral clusters.

The coordination of ions depends on both the dimensionality and the location of the ion, whether within or on the outside of the cluster. For internal ions the coordination number is two for 1D structures and typically three for 2D structures and four for 3D structures. For external ions the coordination number is typically reduced by one for 1D and one for 2D and 3D closed structures if the ion is not connected to an internal ion. Moreover, the coordination numbers may decrease further in hybrid structures, where the dimensionality of constituent fragments is preserved. For example, only one end of a stick (or dangling bond) could be connected to a closed 2D or 3D fragment, but, as we will report below, this configuration is unlikely, and handles⁶¹ are a more common feature in which

fragments of 2D rings are connected at both ends to a 3D fragment. (A handle can be considered as two polygonal faces with more than two ions shared, rendering the 3D bubble a hybrid structure. Likewise, a stick can be formed from a handle in a hybrid structure by folding the handle so that some, or indeed all, of the ions are merged. The same analysis, i.e., the collapse of dimensionality, can be applied to isolated rings.)

The bubble structure is one key class of 3D structures in which there are no internal ions. Closed bubbles are defined as those that contain only tetragonal and hexagonal faces; an octagonal or larger face would constitute a hole, making the structure open. We further define a subclass of perfect bubble structures, where all ions have a coordination of three, as they are of particular importance to ZnO. Perfect bubbles can be both closed and open structures, and not all closed bubbles are perfect, as four coordinated external ions are possible. To understand connectivity in perfect bubbles, we can use Euler's rules (see, for example, Spanó et al.^{62,63} in their structural analysis of the most stable clusters of zinc sulfide) which states that a perfect closed bubble has four tetragonal faces and $(n - 4)$ hexagonal faces for $(\text{ZnO})_n$. Furthermore, these rules also relate the change in these numbers for open bubbles, in particular, for every octagonal face an additional tetragonal face would appear and two hexagonal faces are lost.

Clusters of Size *n* = 1–4. All GM and metastable configurations found using our EA for $n < 4$ are shown in Figure 1a. For $n = 1$ there is obviously only the one structure, a linear stick with length 1.61 Å (RM) or 1.70 Å (SM) and with an energy of formation $E_f = -29.35$ eV/ZnO (RM) or -30.90 eV/ZnO (SM). For $n = 2$, there are only two structures: a linear stick, 2b, with $E_f = -32.53$ eV/ZnO and outer/inner bond lengths of 1.66 and 1.82 Å, and the GM structure, which adopts the structure of a tetragon (rhombus), or two-membered ring, 2a, with $E_f = -34.37$ eV/ZnO, bond lengths of 1.78 Å and Zn–O–Zn bond angles of 88.0°. When the model includes anion polarizability, however, the linear stick, which has an energy -33.31 eV/ZnO and bond lengths of 1.70 (Zn-terminated end), 1.82, and 1.73 Å (O-terminated end), is found to be unstable. Thus, there is only one stable structure for $n = 2$, the ring 2a shown in Figure 1b, with $E_f = -35.36$ eV/ZnO, bond lengths of 1.86 Å, and Zn–O–Zn bond angles of 81.3°.

For $n = 3$, six configurations were generated by the EA. Two were more readily found: a hexagon, or three-membered ring, 3a, with bond lengths of 1.762 Å and Zn–O–Zn bond angles

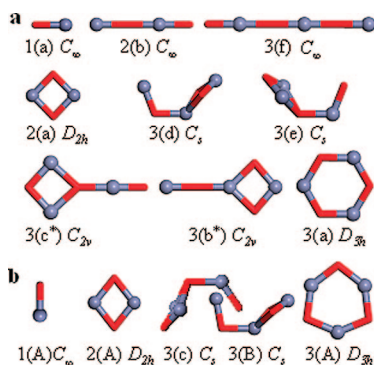


Figure 1. Cluster structures generated using the EA for $n = 1\text{--}3$, when employing (a) RM and (b) after refinement using the SM.

of 119.7° , and a linear stick, 3f, with bond lengths of 1.67 (outermost bonds), 1.79, and 1.70 Å (innermost bond). In fact, of the 200 structures in the final ten populations, 102 were rings, and 60 were sticks. The ring structure, with $E_f = -36.19$ eV/ZnO, is more stable than the stick, with $E_f = -33.97$ eV/ZnO. For both $n = 2$ and 3, the difference in E_f between the ring and the stick is slightly more than 2 eV/ZnO, and the average bond length for the sticks is smaller than that in the ring. By combination of 1a and 2a, two more structures can be constructed in 2D, where the single coordinated ion is either a cation or an anion, respectively. These structures, with values of E_f of -34.27 and -34.25 eV/ZnO, are saddle points on the energy landscape. Strangely, when these structures, 3b* and 3c*, are folded (so that the terminating ion remains coplanar with the 3 other ions on the mirror plane) to create the 3D metastable configurations 3d and 3e, in both cases E_f increases to -34.20 and -34.20 eV/ZnO.

Other clusters with $n = 2$ and 3, considered in ref 41, namely, structures labeled “2(b)” (formed by two $n = 1$ ground-state clusters) and “3(b)” (a ladder structure) in Figure 1 of ref 41, were not produced by our EA, as these structures are neither stable nor saddle points (they relax immediately to the GM structures). By use of the SM, only the ring, cation-, and anion-terminated 3D structures are stable, with $E_f = -37.03$, -35.20 , and -35.18 eV/ZnO, respectively. As a result of the refinement of the ring structure (allowing the oxygen ions to polarize) the bond lengths stretch to 1.81 Å, whereas the Zn–O–Zn bond angles decrease to 105.8° .

The structures found by the EA for $n = 4$ are shown in Figure 2a. The GM structure for the RM is a ring with $E_f = -36.79$ eV/ZnO, and so far, our predicted GM structures agree with those previously reported.^{37,40–43,48} The cuboid, or double twining, is 0.49 eV/ZnO higher in energy than the ring and was also predicted to be the next lowest energy configuration.^{40,41,48} The cuboid is the first possible cage, or bubble, structure, where all ions have a coordination of three. The 2D structure, comprising a tetragon and hexagon that are edge sharing has one imaginary mode of vibration; so the next metastable structure is 4d, which can be visualized as three face-sharing hexagons, each folded along the central axis of the cluster. Six clusters found, 4e*, 4f*, 4 g, 4 h, 4j and 4k, have the same connectivity. As found with $n = 3$, the planar configurations, 4e* and 4f* are saddle point structures that are lower in energy than the folded meta-stable structures. The highest energy metastable configuration, found by the EA, was the linear stick, 4n. Other possible structures that contain more than one singly coordinated ion, such as that labeled as 4* in Figure 2a, were not found in the final populations: the configuration that is likely to be the most stable of the structures with two one-coordinated

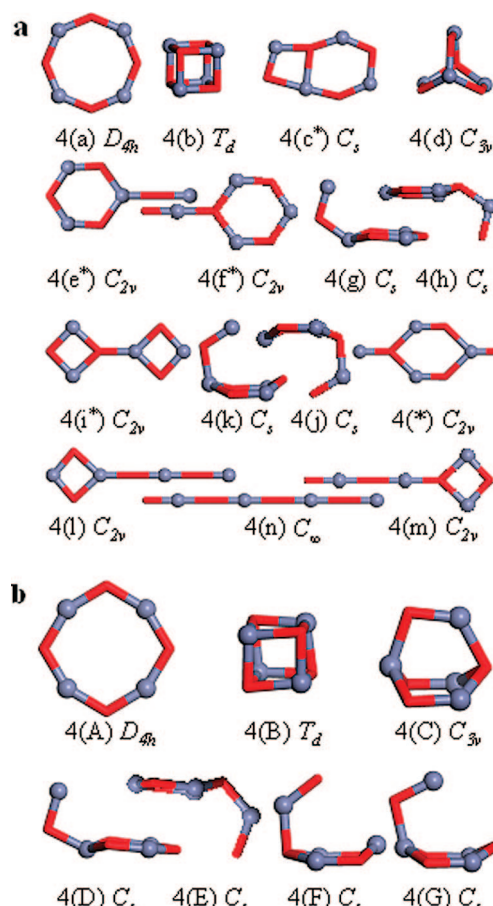


Figure 2. Cluster structures generated using the EA for $n = 4$ when employing (a) the RM and (b) after refinement using the SM.

ions, 4*, has three imaginary vibrational modes and is 2 eV/ZnO higher in energy than the linear stick.

For structures 4b to 4n, the difference in the energy of formation from the GM is 0.49, 0.65, 1.23, 1.37, 1.38, 1.44, 1.45, 1.47, 1.56, 1.56, 1.99, 2.00, and 2.02 eV/ZnO, respectively. Out of these, the SM predicts only six meta-stable configurations with an energy of 0.41, 1.01, 1.22, 1.23, 1.30, and 1.32 eV/ZnO higher than the GM structure, which is still the ring, where $E_f = -37.46$ eV/ZnO. These structures are shown in Figure 2b. As the linear cluster is not stable, we can already assume that larger sized rings will also be less stable and that, with increasing n , eventually the ring motif will be unstable. Furthermore, we have investigated the vibrational modes of the predicted clusters in order to confirm their stability, and indeed, the calculated softening in the lowest (nonzero) frequency phonon mode of the rings as n increases indicates the decrease in stability of larger sized rings. However, although composed of more highly coordinated ions, the cuboid remains less stable than the ring, probably due to the close separation of like-charged ions; indeed, it has been suggested²⁰ that the stability decreases with the number of edge-sharing tetragons in the wall of the cage. We note that larger-size cages will also contain hexagons; 4C has an average coordination number of 2.25, whereas for the other higher energy structures it is 2.00.

Clusters of Size $n = 5$ and 6. Fifteen metastable and four saddle-point structures were generated by the EA for $n = 5$; all are shown in Figure 3a. Again, as reported by others,^{37,40–43,48} the GM is predicted to be a ring (for the RM $E_f = -37.07$ eV/ZnO). Of the top six structures, two can be visualized as “baskets,” 5b–5f, and three as “armchairs,” 5c–5e. As with

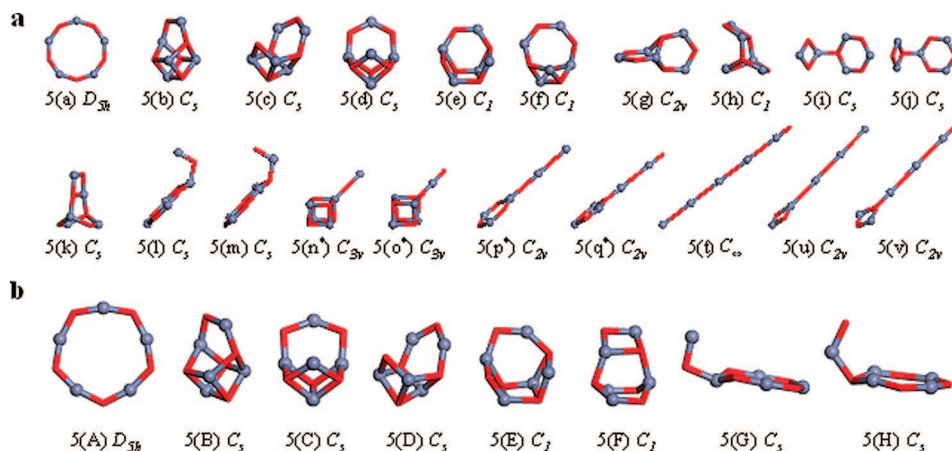


Figure 3. Cluster structures generated using the EA for $n = 5$, when employing (a) the RM and (b) after refinement using the SM.

all ZnO clusters, there is a possibility of generating a second configuration by interchanging species (all cations and anions are swapped); after relaxation, 5c, 5i, 5l, 5n, 5p, and 5u become 5d, 5j, 5m, 5q, and 5v, respectively. We note that clusters with a Zn-terminated ion are typically slightly more stable than the equivalent cluster with an O-terminated ion. Cluster 5g is probably the least likely configuration to be found by construction, showing the value of the EA search; it has an interesting structure that can be visualized as two hexagon rings split down two sides and fused together to create a tetragonal ring. The linear cluster has been labeled 5t rather than 5r as, during the search, fragmentation of the largest sized cluster is possible to ring 4a and stick 1a or ring 3a and ring 2a, as they are more stable, and, therefore, were found in the final population. 5b, 5h, 5k, 5n, and 5o are essentially cluster 4b or 4d fused with an additional stick, 1a, at different sites. For example, the unstable configurations 5n and 5o have a stick 1a along the line of the long diagonal of the cuboid 4b. As before, clusters with the same connectivity but with differing symmetry were found (metastable structures, 5l and 5m, could be obtained by folding the corresponding unstable 2D configurations, 5p and 5q, for example), although not all corresponding 2D configurations, i.e., those for 5i and 5j, were present in the final populations of our statistical ensemble. Fortunately, when n is much larger, these and the other higher energy structures that can be generated for $n = 5$ are filtered out by the EA. Moreover, the six lowest energy structures were present in all final populations (twenty structures each) in the statistical ensemble.

After refinement of the $n = 5$ structures, shown in Figure 3a, we predict only the eight SM structures shown in Figure 3b to be either the GM or metastable. Thus, the change of model has led to eight of the previously metastable structures becoming unstable, and the order of stability has changed for two metastable structures (5c and 5d become 5D and 5C), although the pentagon, or five-membered ring, is still the predicted GM structure. The Zn–O–Zn bond angles are more acute for the SM calculations. As mentioned above, the metastable configurations increase in average coordination with decreasing energy, i.e., increased stability, e.g., 5H to 5B, although this trend may not always hold true: of the eight structures found, the GM structure has the lowest average coordination, and 5a, 5k, 5n, 5o, and 5t are exceptions to this trend.

Curiously, the linear cluster, 5t, has a lower energy than a stick that is terminated by a two-ring structure, 5u and 5v, but higher than a stick terminated by a hexagon, 5p and 5q. Given that rings are more stable than sticks, one might expect that linear patchworks composed of rings and sticks would typically

be lower in energy than the linear stick, 5t. Considering the possible clusters composed of a hexagon ring and stick(s), we find E_f increases with the magnitude of the resultant dipole (i.e., a stick that is terminated at one end by a hexagonal ring had the lowest dipole and required energy). For the clusters composed of a tetragonal ring and stick(s), our calculations predict greater stability when the tetragonal ring is terminated at one end of the stick (by 4.4 eV), despite having a higher dipole (approximately 3 times higher) than when the tetragon is embedded within the stick. Since one tetragonal ring increases E_f then, not surprisingly, two (noninteracting) tetragonal rings increase E_f still further. In this context, we also constructed similar rodlike structures where additional ions are added to the stick so that the separation of two nonterminating rings could be studied, i.e., we considered a class of clusters with increasing n . However, as there can be a favorable interaction between rings (where one has oxygen ions, the other zinc ions, off the axis of the stick), it is possible to construct two members of this family of structures where E_f is lower than that for the linear stick; the smallest sized clusters, $n = 4$ or 5, where rings terminate both ends of the stick (the beneficial interaction between rings is too weak for larger sized clusters).

From the candidate structures within the final populations generated by the EA for $n = 6$, we found 26 unique structures, all stable or metastable. The double ring, or right hexagonal prism, with an energy of formation of -37.34 eV/ZnO, is predicted to be the GM for the RM calculations. So far, for $n < 7$, this is the second structure to be found where all ions have a coordination of three. Structurally, it can be considered as a drum (short cylinder) or the second smallest bubble (cage). The ring structure, which is the structural motif and shape, adopted by the smaller sized clusters $n = 2, 3, 4$, and 5, is the lowest energy metastable structure, with an energy of 0.22 eV/ZnO higher than the GM. Previous reports predict, for $n = 6$, the ring to be the GM^{37,40–43,48} and the double ring as the next most stable structure,^{40,41,48} whereas, even after changing from RM to SM, the double ring remains our GM.

Figure 4a shows that structures 6c, 6d, 6e, and 6k can be created by prying open, by differing degrees, the GM structure, 6a. Interestingly, of these, the 2D cluster, 6d, is not the highest energy configuration, even though it has the least number of Zn–O bonds and largest Zn–O interatomic distances; moreover, it is stable, unlike most other 2D networks of polygons (e.g., the $n = 5$ cluster composed of two hexagons that are edge sharing). Furthermore, after refining 6d we obtain 6G, which is reported elsewhere^{40,41,48} as the second lowest energy metastable structure. The enlarged bond angles (previously ca. 90°), of the

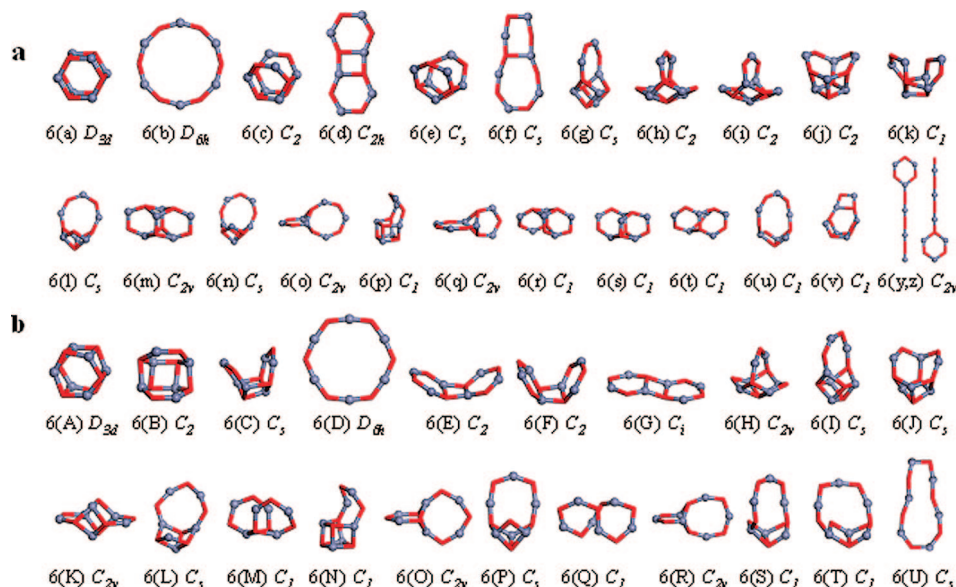


Figure 4. GM and metastable configurations found using the EA for $n = 6$, when employing (a) the RM and (b) after refinement using the SM.

other pried open hexagonal prisms, are roughly 115° , which is a little smaller than the 120° angles of a regular hexagon. There is also a range of metastable clusters, 6m (also reported by Jain et al.⁴¹), 6r, 6s, and 6t, which can be orientated to reveal edge-sharing hexagons. Thus, although three-body potentials were not employed, the RM predicts an increase in stability if hexagonal features are adopted.

Again, we have isostructural pairs, e.g., 6h and 6i, 6l and 6n, 6r and 6s (defective versions of 6m), 6o and 6p, and 6y and 6z, which have a difference in E_f of 0.007, 0.015, 0.009, 0.026, and 0.005 eV/ZnO, respectively. Surprisingly, isostructural pairs with the smallest change in energy, 6h and 6i and 6y and 6z, are those where the coordination number of Zn differs from that of O; therefore cluster pairs with the largest difference in energy must have a greater degree of relaxation after interchange of species. This effect can be confirmed by comparing 6L with 6P and 6O with 6R in Figure 5b, where we note that the anions occupy the corners of the largest ring, whereas the cations are on the sides of this ring. The isostructural partner for 6j was not found during the 10 runs of the EA for $n = 6$. Modeling this missing cluster, we found that the RM predicts that it is a saddle-point structure with E_f 0.01 eV/ZnO higher than that for 6j. Moreover, to locate this structure by relaxing 6j after interchanging species, a smaller step size used in the optimization routines was necessary; otherwise a different structure was found. The fact that the final populations do not contain any more saddle-point structures is an indication that the $n = 6$ energy landscape is sufficiently complex compared to the landscapes previously probed; that is, using the same number of EA cycles and population size, the search over the smaller landscapes was sufficient to reveal saddle points. The linear cluster for $n = 6$ was also missing from the final populations. Fortunately, high-energy and saddle-point structures on the energy landscape defined by the RM are not expected to be important.

Clusters of Size $n = 7, 8$, and 9 . For $n = 7$, 7a and 7f can be visualized as $6a + 1a$, with the nearest bond parallel to the additional stick being broken, within the hexagonal ring of the drum for the former and connecting the hexagonal rings for the latter. The resulting structures are shown in Figure 5. As with the drum, by breaking more bonds between the hexagonal

and octagonal faces of 7a (a chair configuration) more metastable configurations can be generated, namely, 7b, 7e, 7h, and 7i. Of these structures, only 7e has been proposed elsewhere^{40,48} as feasible. In fact, although structure 7a has been proposed as the GM for other binary compounds, e.g., zinc sulfide,⁶¹ silver iodide,⁶⁴ and magnesium oxide,⁶⁸ we have not found it reported by others for zinc oxide. The other structures that have already been reported as metastable include 7c and 7f (as 7h and 7f by Wang et al.⁴⁸) and 7i (as 7b by both Maxtxain et al.⁴⁰ and Wang et al.⁴⁸).

For $n = 8$, the right octagonal prism (drum), or double four-membered rings, is found to be the second most stable structure, and, again, by prying open the two largest (this time both octagonal) faces, several other metastable configurations are generated, for example 8c, 8e, and 8f. The octagonal drum is one of two different bubble configurations for $n = 8$, where all the ions are 3-fold coordinated; the other is the GM, which is composed only of tetragons and hexagons as shown in Figure 5. We note that configuration 8m has two ions with a coordination number of two. Likewise, the GM for $n = 9$ is a bubble comprised of tetragons and hexagons, which agrees with previous studies.^{40,43} Configuration 9b, comprised of three hexagonal rings to form a barrel, is 0.09 eV/ZnO (0.38 eV/ZnO for the SM) higher in energy than the GM, even though it contains six four-coordinated ions. This observation points to the greater stability of tetrahedral and trigonal compared to tetragonal coordinations for ZnO clusters. However, we note that previous studies^{40,43,48} report 8B to be more stable than 8A, and Wang et al.⁴⁸ predict a 2D network, octagon–tetragon–octagon—and the barrel, 9b, to be the GM for $n = 8$ and 9, respectively. The search for $n = 9$ also produced enantiomers (9c, 9d, and 9e, labeled with “ $\times 2$ ” in Figure 5) and octagonal chair structures (9e and 9k) analogous to that of 7a.

In the sequence of clusters considered so far, the relative stability of the 2D rings has fallen with increasing n : for $n = 7$, the ring structure has slipped to fourth place (7d) in direct contrast to previous studies^{37,40–43,48} that report the 2D ring as the GM structure. Moreover, rings are no longer found within our final statistical populations that were generated when we searched the landscape for larger sized clusters, i.e., there are an increasing number of 3D structures that are more stable than

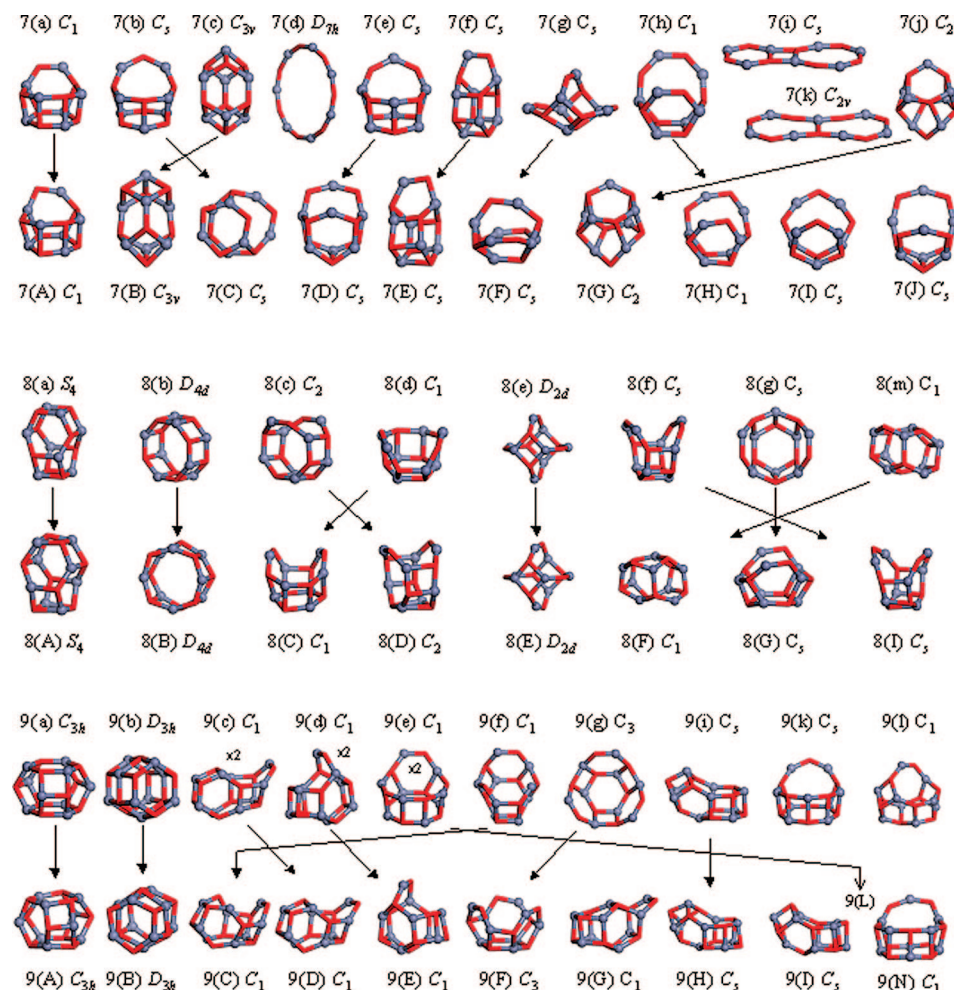


Figure 5. GM and metastable configurations found using the EA for $n = 7\text{--}9$. Arrows indicate the genealogical connection between the structures obtained with the rigid ion model and after refinement using the shell model.

the alternative 2D structures. However, for $n = 7$, perfect bubbles, where all ions are 3-fold coordinated, are not yet the most stable motif. The imperfect bubbles can be visualized as containing handles, where, by definition, the handles are made up of two coordinated ions.⁶¹ By consideration of the energy per ZnO monomer unit, we note that the stability of the infinite linear stick is less than that of the hexagonal sheet, which is in turn less than that of the bulk (wurtzite, for example). Thus, it is no surprise that as n increases, rings, which are bent fragments of the infinite linear stick, become less favorable than bubbles (bent fragments of the hexagonal sheet). As previously shown for sub-nanoparticles of ZnS,⁶¹ as handles are themselves fragments of the rings, the stability of a configuration will fall as the number and the length of handles increases. However, just as the stick and rings are the most stable configuration for $n < 6$, the chair, which contains a handle containing two ions, is the GM for $n = 7$, even though there is a perfect bubble, or “clam,” configuration, 7c. When the SM is employed, the clam relaxes to a more stable configuration than that of 7b, which contains a three-ion handle, but remains 0.23 eV/ZnO less stable than the chair. As n increases, we will find that the final populations of our EA will have fewer structures containing handles.

It is useful to consider the GM and metastable clusters ordered by energy like rungs of a ladder, with the GM occupying the lowest rung. The key structures found for $n = 7\text{--}9$ are arranged in Figure 5 so as to emphasize the changes in the order of stability when changing models (RM to SM calculations).

Generally, there are few examples where there is a large change in the order of stability, at least greater than one rung, particularly for low energy clusters (near the GM, or lowest rung of a ladder). Employing of the EA to search the RM, as opposed to the SM, landscape is much faster and appears to provide the desired key structures on the SM landscape. However, there are some changes, and so it is important not just to locate the GM on the RM landscape but also low energy metastable configurations. Although we are less concerned with structures moving up the ladder (i.e., decreasing in stability), e.g., the 7a ring structure which moves up to 7P, the three examples where there is a large drop down the ladder are a warning, particularly 9f, which becomes the third most stable structure for $n = 9$ by moving four rungs. Therefore, for larger n , we continue to locate at least the top eight (meta)stable structures.

Clusters of Size $n = 10\text{--}32$. In Figures 6, 7, and 8, we show key structures, which include our predicted GM structures, for clusters of size $n = 10\text{--}32$. There is generally a good match between the GM structures reported here and previously, and, importantly, where discrepancies occur, previously reported GM structures are still found within two rungs away from our GM. Matxain et al. and Wang et al., who investigated structures up to $n = 15\text{--}18$, respectively, report our 10B, 11A, 12A, 13A, 14A, 15A³⁷ and 10A, 11A, 12A, 13C, 14A, 15A, 16A, 17B, 18A⁴⁸ as GM. We have also compared our structures to a number of other studies, where GM structures have been reported for a selection of n : 10A, 11A, 12A, 13B, 14B, 15A,

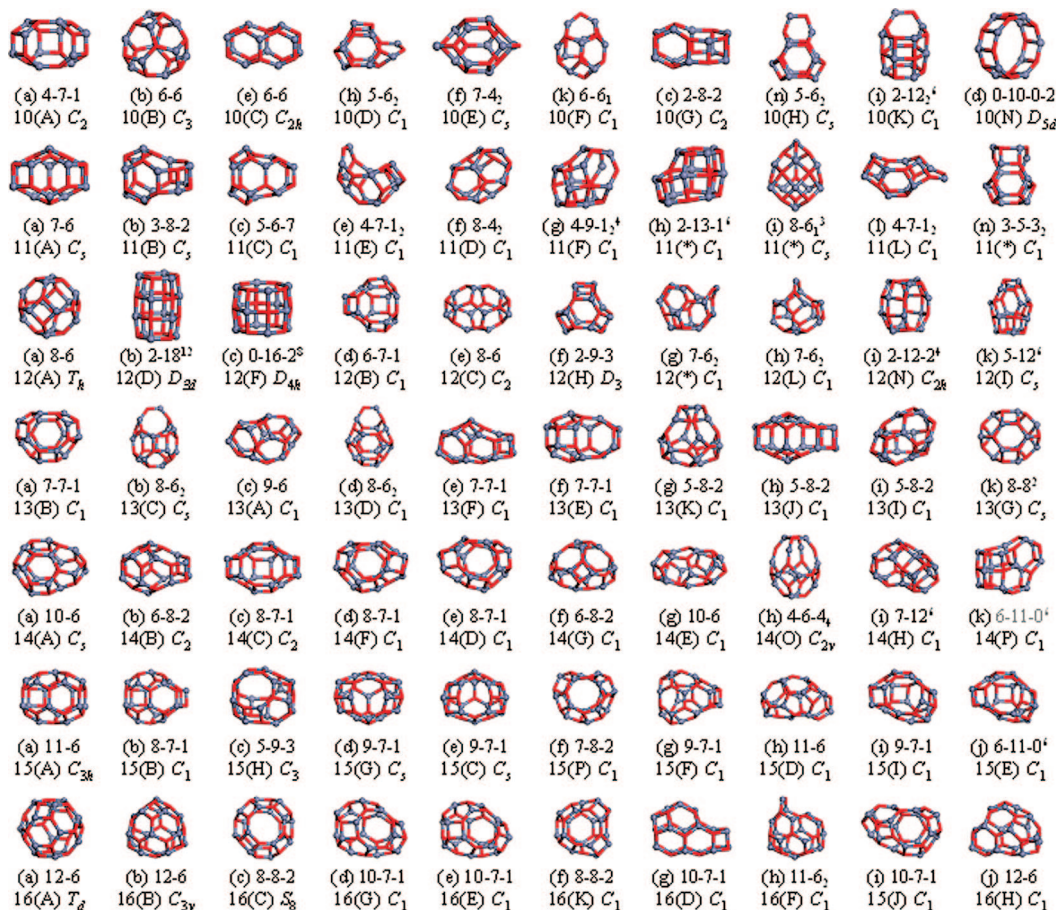


Figure 6. GM and metastable configurations found using the EA for $n = 10-16$. The nomenclature is explained in the text.

16A, 17A, 18A, 21A (Reber et al.⁴³), 10B, 12A, 16A, 20B, 24B (Zhao et al.⁴⁴), 12A, 16A, 28A (Zhu et al.⁴⁶), and 24C, 28A (Wang et al.⁴⁹). In their study, Wang et al.⁴⁸ also report metastable structures, which include (listing them in decreasing stability) 10B, 10C, 10N, the barrels 12F followed by 12D (i.e., in the opposite order to us), 16B, 16C, ?, 18B, ?, 18C, 24A, ?, 24B, 24R and 28C, ?. Here, the question marks indicate the cluster structures that we had difficulty in identifying. The comparison of our generated structures to those shown in figures reported in previous studies becomes more difficult as n increases, especially when symmetry is low. Therefore, as the structures have become more complex, we have introduced a new nomenclature: each configuration is labeled $i-j-k-l-p,q$ to indicate it has i, j, k , and l hexagonal, tetragonal, octagonal, decagonal faces, respectively, as well as p four-coordinated ions and q two-coordinated ions (and, if no confusion results, k, l, p , and q are not stated if they take the value of zero). So, for example, 10C, which is labeled 6–6, has six hexagonal and six tetragonal faces, whereas 10d, which is labeled 0–10–0–2, has two regular decagonal and ten tetragonal faces. In our nomenclature, handles are removed and typically replaced by a bond, when composed of an even number of atoms. In doing so, from the labels, it is more apparent if a structure can be created by an addition of a Zn–O stick or unit. For example, 10K is composed of 11 tetragons, 1 hexagon, and 2 octagons but is labeled 2–12⁶, thus indicating that it can be built from 1A (a linear stick) and 9B (which contains 2 hexagons, 12 tetragons, and 6 four-coordinated ions, that is 2–12⁶).

From the structures shown in Figures 6–8, we note that, as n increases, the particles are less likely to contain handles and that the bubbles contain only ions that are 3-fold coordinated,

as opposed to four, especially for the SM calculations. Moreover, the bubbles are typically formed from hexagons and the inclusion of larger polygons results in additional tetragons if the coordination of all ions is to remain three (Euler's rule⁶²). One exception is found for $n = 10$, where the GM contains an octagonal face, in a 4–7–1 arrangement as opposed to 6–6. We suggest that size effects play a crucial rôle here; as a 6–6 arrangement, 10B is preferred for ZnS where the bond lengths are longer, and hence the diameter of the bubble is greater.⁶¹

Many of the structures found can be visualized as a cut from two identical, parallel polygonal sheets that have been inflated so that a fraction of the interlayer bonds are broken (so that ions become 3-fold coordinated). The GM for $n = 11$ is one such example: in Figure 6, when 11A is viewed from above, a patchwork of two hexagons and one tetragon is seen. Further examples include those listed in Table 2. 14P can be described as the barrel configuration 9B merged with double drum (or binocular) configuration 10C. It provides an example of where the two layers (two hexagons and three tetragons) are only partially separated (one of the internal interconnecting bonds remains unbroken with the length of 2.05 Å) and the cluster also has six four-coordinated atoms around the center of the barrel. In counting the faces, we ignored the internal bond and treated the deformed octagonal face as an edge-sharing tetragon and hexagon, since from above it appears that it is missing a bond (in fact the interatomic separation distance is 2.64 Å) across its face (along the line of the fold, across the top of the cluster).

Considering the configurations for $n = 10$, we find that on switching models from the RM to the SM, the rank of configurations containing larger polygons generally becomes

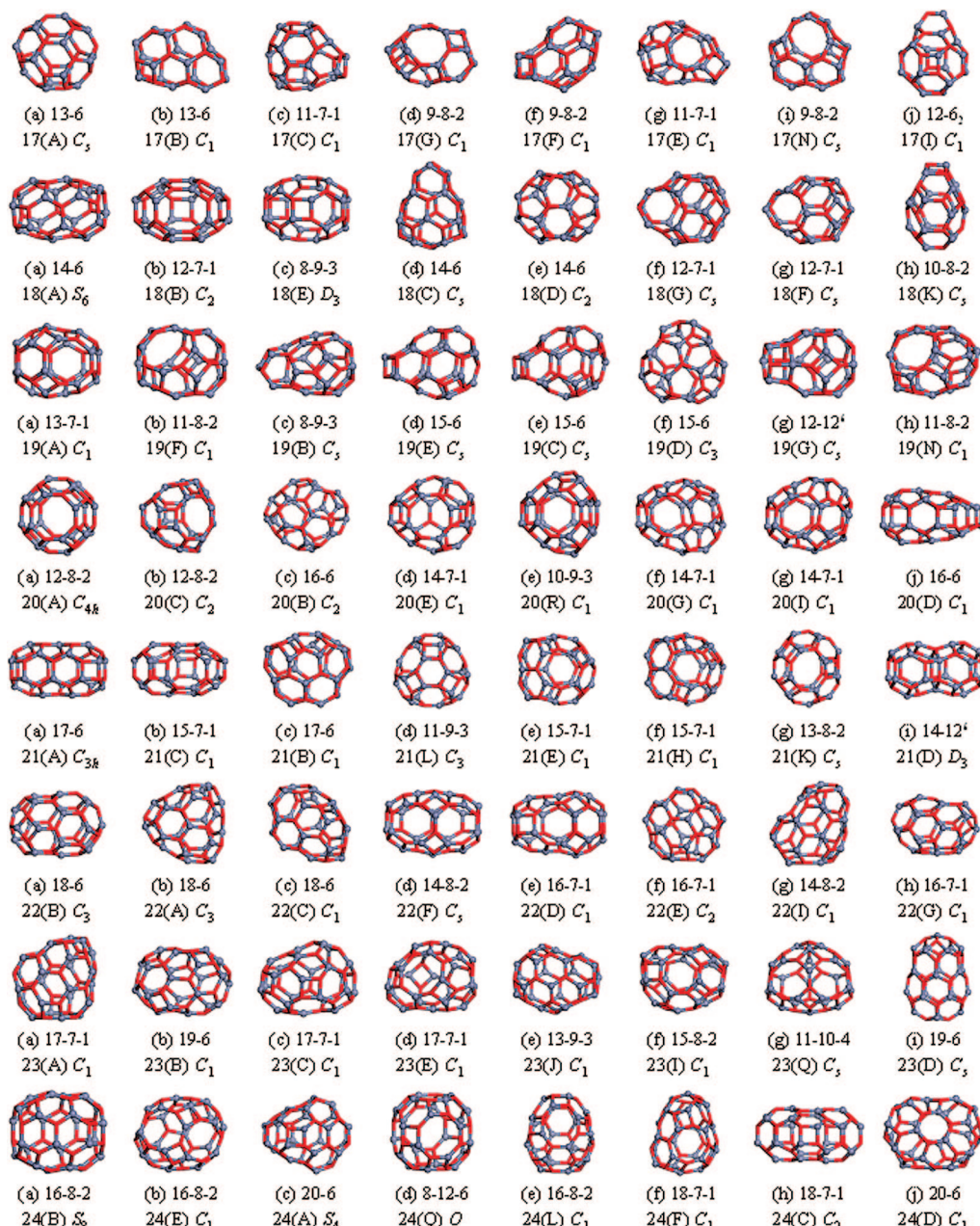


Figure 7. GM and metastable configurations found using the EA for $n = 17-24$.

worse, as noted above; for example, 10c and 10d, the first containing two octagons and the latter two decagons, become 10G and 10N, respectively. The GM, or “ashtray” configuration, 10A is also reported to be the GM for silver iodide⁶¹ and magnesium oxide.⁵² By addition of a stick to 10A, we can generate either of the two metastable configurations, 11E and 11L. In our figures, we have typically omitted one of each pair of structural isomers (a pair of 14d and 14e is one exception) and configurations that are similar to one already shown. For example, 11d, not shown, has the same connectivity as 11c but somewhat different bonds lengths and angles, particularly around the octagonal face, and both relax to 11C when the SM is employed. 11i and 11k are structural isomers where one anion and one cation, respectively, have a coordination of four.

Where a compound forms bubble structures, the sodalite cage, 12a or 12A for $(\text{ZnO})_{12}$, appears always to be adopted as the GM structure for $n = 12$. Behrman et al.³⁸ have highlighted the sodalite cage as a possible magic number structure and have investigated the stability of this structure for a whole range of

binary compounds.³⁹ The dominance of sodalite can be explained if we consider the energy difference found between 12a and 12b (a barrel formed from aligning four hexagon rings), which is 2.19 eV (and 2.47 eV for SM calculations), or between 12A and 12B, which is 2.16 eV. These are large compared to the values obtained for other sized clusters; see for example Figures 9 and 10, where the energy of formation (RM) for the lowest seven configurations for each cluster size ($n = 12-32$) and the energy difference between the lowest two is plotted as a function of n . For $n = 13$, all 20 candidates found were within 2.19 eV of our predicted GM structure. Moreover, the EA easily generates the sodalite configuration with a 100% success rate, see Table 3.

Many structures were found to be structural isomers, for example, 12E, originally 12j and not shown, is the structural isomer of 12L(h), a basket configuration containing a handle. Other examples include: 13K(g) and 13I(i), 14F(d) and 14D(e) with an energy difference of less than 0.1 eV, 14H(i) and 14I(j), 15G(d) and 15C(e), 15I(i) and 15E(j), 16G(d) and 16E(e), 16N(l) and 16

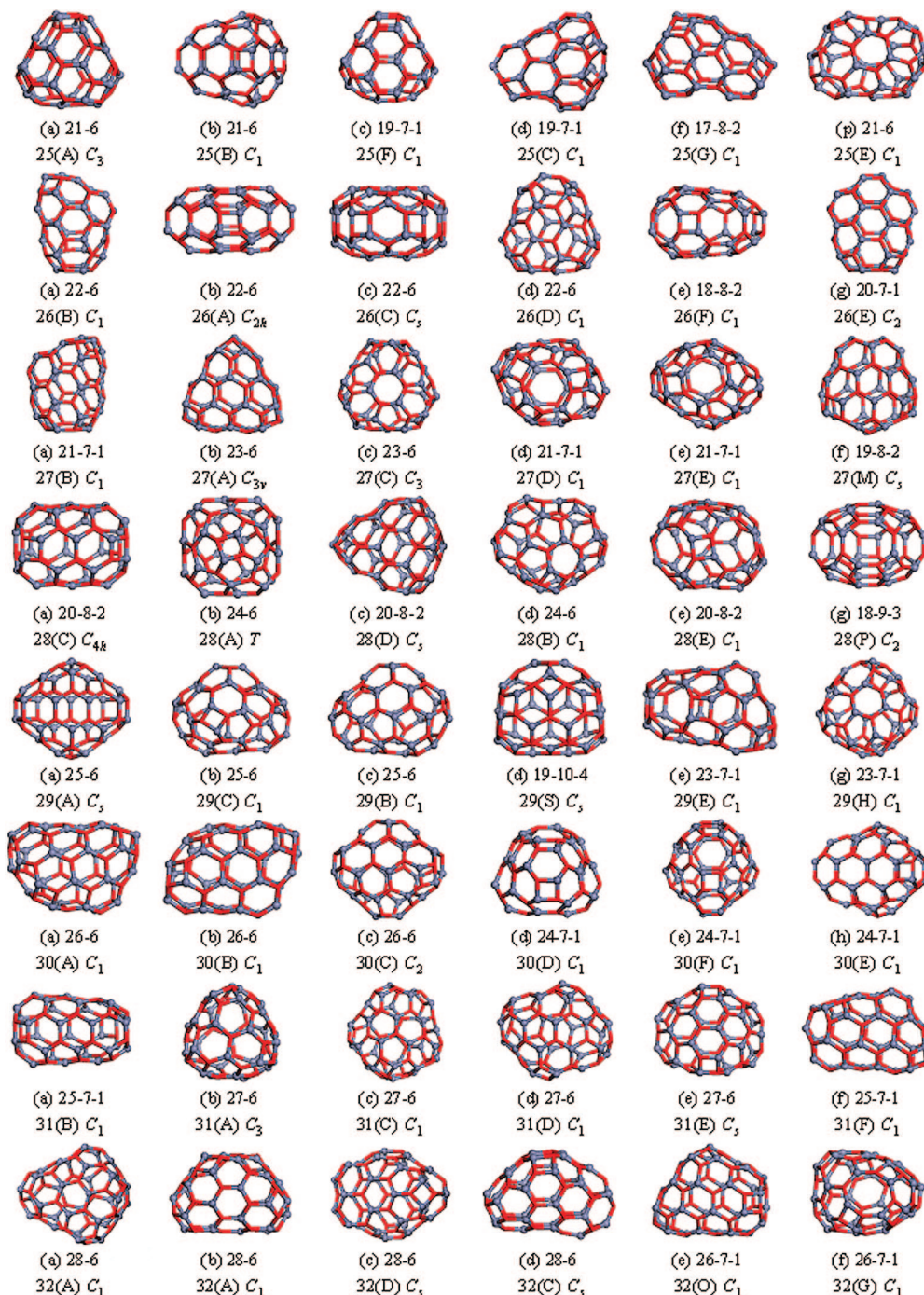


Figure 8. GM and metastable configurations found using the EA for $n = 25-32$.

$L(n)$, 17C(c) and 17D(e), 17E(g) and 17H(h), 18F(g) and 18G(f), 19C(e) and 19E(d), 20G(f) and 20I(g), 23C(c) and 23E(d), 24G(g) and 24I(h), 25C(d) and 25D(e), 27E(e) and 27F(f), 28E(e) and 28G(f), 29B(c) and 29C(b), 30G(f) and 30H(g), 32E(d) and 32D(e), and 32H(g) and 32G(h). Changing from the RM to the SM, we typically find that the relative ranks of the isomers swap. Many structures were also found to be enantiomers (left and right hands have the same energy of formation and, for the purposes of ranking, each pair is counted only once): examples include 14D, 14F, 14H and 14I, 15E and 15I, 16K and 17E, and 17H.

As discussed later, we can assess the relative stability of a particular size GM structure by plotting the nucleation energy, $E_n - (E_{n-1} + E_1)$ as a function of n , i.e., we compare the energy of formation of neighboring GM clusters after adding the energy

of formation for the 1A stick. Many metastable clusters can be constructed by addition of 1A to a neighboring size GM or metastable cluster, which perhaps provides a nucleation route. Rather than addition of 1A, the construction of metastable clusters found by the EA can also be achieved by adding 2A (the smallest ring) or 3A: starting from 11A, 13E and 13F are two such examples of clusters of the former, and the chiral 14H, and its enantiomeric partners, 14I, are examples of the latter. Another example is 19G, which is 12A + 3A, a sodalite cage face sharing with the drum (6A). Some metastable clusters can be described as constructed from identical smaller GM units that are face sharing, for example, 21D as two face sharing sodalite cages (12A), or 9B and 10C as two face sharing drums (6A).

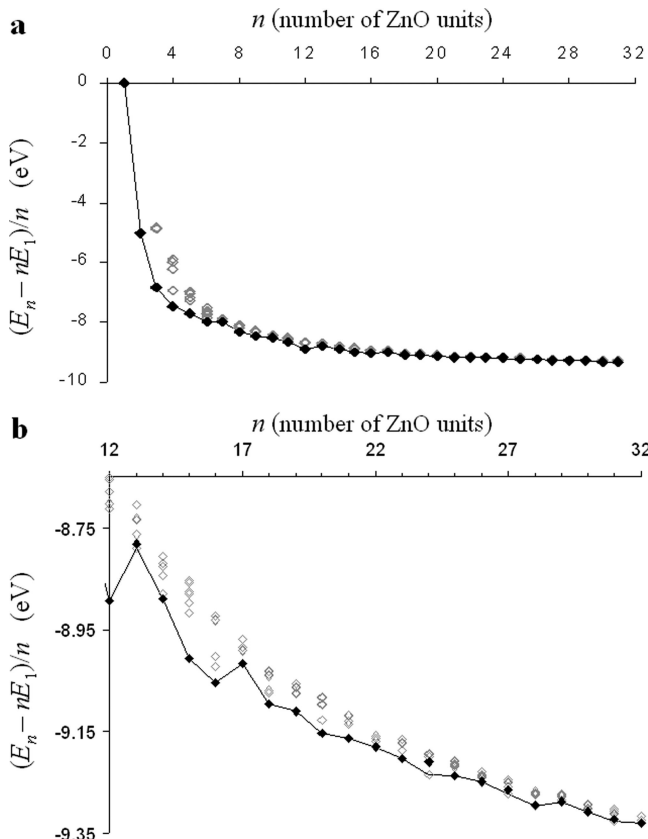


Figure 9. Energies of formation of ZnO clusters per formula unit using the RM for (a) the full range investigated and (b) larger clusters for which the density of points is higher. Seven lowest energy points are shown for each cluster size; the line joins the GM structures, and the solid diamonds indicate the GM cluster after refinement using the shell model.

TABLE 2: Contents of the ZnO 2D Patchworks that Refine to GM and Metastable Structures

sluster	T	H	cluster	T	H	O
10C		2	19A	3	4	
14A, 14C	1	3	22I	3	5	
17B	1	4	24C, 24M, 25G	3	6	
19B, 20D	1	5	27B, 27C	3	7	
22E	1	6	20A	4	4	
24B	1	7	23J	4	5	
16D	2	3	28C, 28D, 28P	4	7	
18A, 18B, 18C	2	4	29S	5	7	
20C, 21A, 21C	2	5	10G	1	1	
23A	2	6	19F	2	3	1
26A, 26C, 26E, 26G	2	7	18E, 18K	3	2	1
28C	2	8	20C	3	3	1
31F	2	9	24R	4	4	1
14B, 27N	3	2	23Q	4	2	2
16C, 17F	3	3	24R	5	2	2

The seven lowest formation energies for the RM, found by the EA, for each cluster size are plotted in Figure 9. Generally, the spread of the top seven energies for each cluster size reduces with an increase in n , which is not surprising, as the number of possible metastable states will also generally increase. The line joins the RM energies of the GM structures, and the solid black diamonds (as opposed to the open diamonds) indicate the GM structures when the SM is employed. We note that the line does not connect the solid black diamonds for $n = 13, 22, 24, 26, 27, 28, 31$, and 32, where there is a change in the GM on changing models. The most noticeable case is at $n = 24, 27$, and 32 and clearly not the smallest clusters (for larger n we

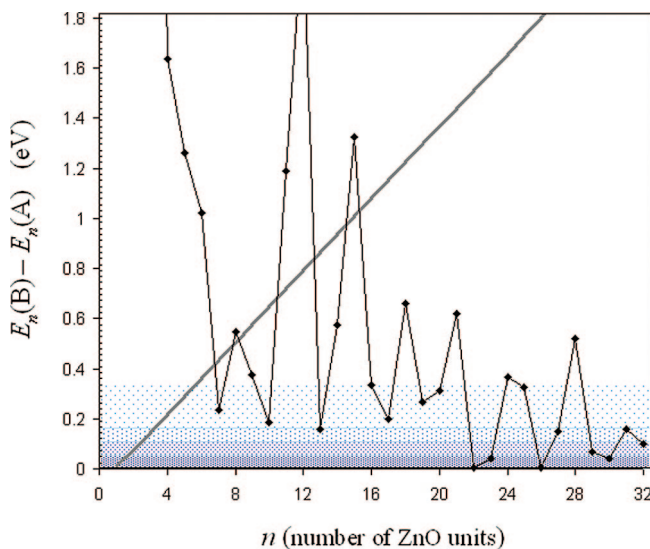


Figure 10. Energy difference between the most stable and second most stable structures plotted as a function of cluster size (shell model). The gray line shows the ambient thermal energy; and the thermodynamically expected 10%, 1%, 1%, 1 ppm abundance bands are filled by dots with a decreasing density.

TABLE 3: Success Rate in Generating the Global and Local Minima (GM and LM) for the Statistical Set of EA Runs^a

<i>n</i>	GM (a)	LM (b)	LM (c)	LM (d)	LM (e)	LM (f)
12	100	80	90	100	100	90
13	100	100	100	100	70	80
14	100	100	100	100	100	100
15	100	100	100	90	80	100
16	100	100	100	100	90	100
17	100	30	10	60	60	40
18	40	100	90	60	70	20
19	90	100	100	50	20	40
20	90	100	80	90	50	50
21	90	50	40	70	100	100
22	100	100	100	50	60	100
23	100	100	100	100	100	100
24	100	10	100	100	60	100
25	100	100	100	30	60	40
26	100	90	100	100	70	90
27	100	60	70	10	100	100
28	90	80	100	70	20	70
29	100	30	70	90	30	10
30	40	40	70	70	100	30
31	50	80	60	50	50	40
32	10	70	80	20	50	40

^a Unexpected low success rates that are discussed in the text are highlighted in bold.

would expect other examples to be less noticeable as the spread in energies decreases). The low energy configurations found for $n = 24$ are unusual as most of them have at least two octagonal faces; other examples include $n = 19, 20, 23, 27$, and 28. Despite containing two octagons, the GM found by the EA for the RM is particularly stable, as it is essentially an eight by two hexagonal sheet that has been neatly rolled to create a barrel with point symmetry S_8 (each end capped by an octagon and four squares). Other examples of barrels, with identical capped ends, are found to be low energy configurations including 16c and 32a (from an eight by one and an eight by three hexagonal sheet) and 20a and 28a (with one capped end rotated about the axis by 45°). Barrels capped with a hexagon and three tetragons are also favorable, particularly with the SM; examples include 15a, 18a, 21a, 24b, and 27d. Barrels are

particularly easy to construct, which we will exploit in a subsequent study, and have also been targeted by others.^{43,49} There are even barrels capped with both types; see configuration 31a. However, octagonal faces are penalized more heavily with the SM than hexagonal faces (large rings are in fact unstable): the greater the number of octagon faces the larger the jump up the ladder (decrease in rank) when switching models, as with the $n = 24$ configurations shown in Figure 7, where configurations contain either 0 (which consequently are promoted down the ladder), 1, 2, or 6 octagonal faces. Structure 24b contains only tetragons and hexagons and becomes the GM for the SM, 0.37 and 0.43 eV more stable than structures 24B and 24C, respectively. Ignoring symmetry or the general shape, a similar explanation can be advanced for $n = 17$ and 32; typically, the bubble-shaped clusters are promoted or demoted depending on whether they have fewer or more octagonal faces. Below, we will discuss the large energy gap between the GM and the lowest metastable configuration for $n = 12$ and 15.

Generally, the GM energies become increasingly negative with increasing cluster size. The rate of change also decreases with n . We note that the GM energies should converge to the energy of bulk ZnO, i.e., -10.46 eV/ZnO. Considering $n = 12\text{--}32$, there are some notable exceptions to the general trend, i.e. local maxima in our predicted GM energy curve for $n = 13, 17$, and 29. Curiously, we note that Bulgakov et al.²⁰ report a local abundance minimum at $n = 13$ within the range $n = 2\text{--}16$ in the ablation plume. If we ignore the lower neighboring GM energies, the GM energies, including 13 and 29, there actually appears to be a gradual decrease, without oscillations, and we conclude that the appearance of local maxima is due to the prominent neighboring local minima: spherical cages with the highest symmetry point groups found, T_h , T_d and T , for $n = 12$ (sodalite), 16 and 28, respectively. Actually for $n = 28$, the RM predicted GM is a symmetrical barrel (symmetry point group C_{4h}), which has a very similar energy of formation to the spherical cage. However, the rank reverses when the SM is employed so that the barrel, which contains two octagonal faces, becomes less stable. We note that Behrman et al.³⁸ predicted 12A and 16A to be magic numbers, i.e., clusters of particular size that are relatively more stable and thus produced in more abundance when synthesized either by nucleation or laser ablation of a surface. Moreover, these GM clusters, including 28, have been proposed to be the origin of magic numbers for boron nitride.⁶⁵

Clusters with higher symmetry tend to be relatively more stable as seen in Figure 11a, where the relative stability, as measured in the SM, of each GM is compared with the average stability of its neighboring sized clusters. In Figure 11b, we show the energy function $E_n - (E_{n-1} + E_1)$, which gives a measure of stability with respect to nucleation (an additional Zn–O unit to each GM cluster). If there is an abundance of Zn–O monomer units, the local minima give a crude indication of which GM clusters are more likely to persist.⁶¹ A similar pattern is found in parts a and b of Figure 11: higher symmetry structures tend to have a lower energy. In both energy functions, the hexagonal ring has a lower value than other sized rings, tetragonal being the next lowest; then from the octagonal ring onward, even higher values are predicted, which indicates that ZnO bubble clusters should maximize the number of hexagonal faces. However, when comparing parts a and b of Figure 11, there is one exception, namely, the GM structure for $n = 16$ (the spherical T_d cage) is not a minimum with respect to nucleation as $n = 15$ (hexagon capped barrel with C_{3h} point symmetry) is relatively more stable than the less symmetric n

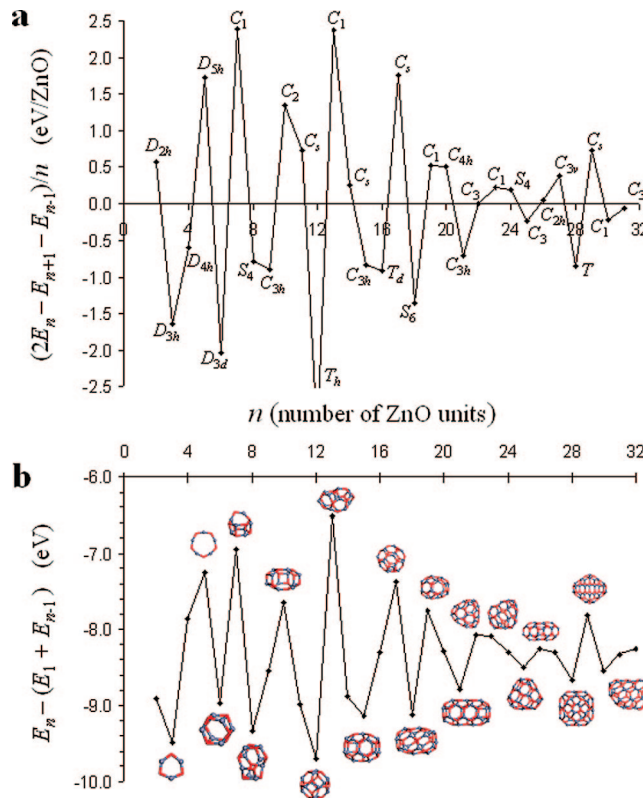


Figure 11. (a) Relative stability and (b) nucleation SM energies plotted as a function of cluster size.

= 14 GM cluster. However, as nucleation is dynamic, in the sense that clusters could also fragment, we could also have considered $E_n - (E_{n+1} - E_1)$, and as $n = 17$ is relatively less stable, the local minimum is at $n = 16$.

In Figure 10, we show the difference between each GM and the lowest metastable structure for each size of cluster. It is clear that $n = 11, 12$, and 15 structures have high values, i.e., they are very stable with respect to other configurations of the same size, greater than 1.19, 2.16, and 1.33 eV, respectively, whereas the energy gap between the GM and the lowest metastable structure is less than 0.7 eV for all other sizes above $n = 6$. The ambient thermal energy (using $1/2k_B T$ per internal degree of freedom) is shown in Figure 10 as the diagonal gray line. Points above this line represent structures that are not accessible by thermal excitation at room temperature. Thus, metastable clusters for $n = 3\text{--}6, 8, 11, 12$, and 15, which includes the cuboid, $n = 6$ ring, and octagonal drum, can be realized only by nonequilibrium processes. One can ascribe this property to either the particular stability of the GM or the instability of the metastable structures. Indeed structures 12A, the sodalite cage, and 15A, the hexagon terminated barrel, are perfect bubbles with a maximum number of hexagonal faces, as found in earlier molecular dynamics simulations,³⁸ and have higher symmetry than other configurations of the same size. In contrast for $n = 11$, as shown in Figure 6, 11A is the only perfect bubble configuration (all atoms three-coordinated) with a maximum number of hexagonal faces.

We have also characterized the expected abundance, at ambient temperature, of low energy structures on thermodynamic grounds assuming the Boltzmann distribution. Within the lowest band, the abundance of the second lowest stable configuration is predicted to be greater than 10%, and thus 22A, 23A, 26A, and 30A are not unique; although the motif of the clusters is still predicted to be bubblelike for each size,

particularly for the bigger clusters examined in this study. For $n = 22A$, $22B$, $26A$, and $26B$ structures are perfect closed bubbles, and interestingly, the negligible energy difference implies both are just as likely. There are points, for $n = 9, 14, 16, 18, 21, 24, 28$, below the thermal gray line and above the highest band where the abundance is expected to be less than 1 ppm, which indicates that metastable structures are very unlikely but still thermally possible.

In Table 3, the success rate in generating each of our predicted six most stable structures for each cluster size is presented as a percentage of ten EA runs with a fixed set of parameters (apart from the number of atoms, which obviously is defined by n). In general the performance of the EA is very satisfactory, especially as in this set of runs we have not changed the parameters to take into account size effects. The first irregularity in the success rates for predicting metastable structures occurs at $n = 17$, whereas for the GM it is at $n = 18$. Although one might argue that it is only important to locate the GM at least once, it is instructive to consider why the EA struggled so as to avoid such problems for the larger sized clusters. The ease of locating a metastable structure (local minimum) depends on the relative width of the basin within which it sits compared to its neighbors, the relative width of the superbasin containing neighboring local minima that are connected by barriers below a defined height or the basin on the relaxed landscape, and the relative width of the supersuper basin etc. Others^{66–68} have employed a technique for such analyses, where the landscape is drawn so that it resembles the roots of a tree, a disconnectivity graph, and from which one can see whether the landscape is likely to funnel the EA toward a local minimum or the GM. These analyses need the knowledge of the barrier heights between the local minima and are therefore beyond our present study. However, by comparing the structures and the energies of the (meta)stable structures we can at least speculate as to why $n = 17, 18, 24, 27$, and beyond 29 have proved problematic to find, particularly the smaller structures. For $n = 17$, we first notice that the difference in energy between 17b and 17c is of the same order as the energy tolerance used to determine duplicate candidates within the current population. 18a is a barrel; moreover other low success rates correspond to barrels (24b, 27d and 32a), so, ignoring one of the exceptions, 21a, we find that spherical bubbles are in general easier to generate. It is instructive to make a direct comparison of the success rate of the EA with that of construction. Ideally, we should target a range of possible shapes, e.g., barrels as well as spherical bubbles. Thus, several EA runs should be performed within spherical and then nonspherical containers for each size, n . Beyond $n = 29$, to improve the rate of success, we need to use at least a larger container (diameter 16 Å, compared to the largest interatomic distance of >13 Å for 27A) and increase the number of EA cycles. Ultimately for larger clusters, the move class operators of EA may need revising, as new topological features emerge so that the single-walled bubbles are no longer dominant; crossover of two bubble structures would readily produce a third bubble structure but not a double bubble, for example. After searching the configuration space using a genetic algorithm for smaller clusters (up to $n = 18$), in a subsequent paper Wang et al.⁴⁹ construct structures for $n = 24, 28, 36$, and 48 based on chemical intuition, where more symmetrical structures are, perhaps, easier to envisage. However, of their 12 reported structures, none has the symmetry point group C_1 for $n = 24$, cf. 24E and 24F (see also 24M) in Figure 7. We stress, therefore, that the EA remains an important

complementary tool for the search of key structures, as unexpected low symmetry configurations may be missed in other approaches.

Summary and Conclusions

In this article, we reported the stable and low energy metastable structures of $(\text{ZnO})_n$ for n up to 32, which includes the first systematic search for this compound above $n = 18$. In locating the GM and metastable structures, we have found structural motifs and building blocks that we intend to utilize in a different nonevolutionary approach, namely, construction. As a function of n , GM and low energy metastable clusters are initially rings and then bubbles that gradually have fewer handles (atoms that are two rather than three coordinated) and nonhexagonal faces. Other findings include: (1) the average bond length for the sticks is smaller than that in the ring; (2) the cuboid (4B), the right hexagonal prism (6A), and the clam (7B) are the first three perfect bubbles; (3) the Zn–O–Zn bond angles are more acute for the SM; (4) a greater stability of tetrahedral and trigonal coordinations compared to tetragonal for ZnO clusters; (5) isostructural pairs with the smallest change in energy were those where the coordination numbers of Zn differ from that of O; (6) when changing from the RM to the SM, the number of changes in the order of stability, of magnitude greater than one, is small (but still significant), and the rank of bubble structures with fewer octagonal faces typically improved; (7) many of the clusters could perhaps have been created by inflating two, topologically identical, parallel layers of square-hexagonal sheets; (8) relative stability of GM clusters was predicted for spheroid cages $n = 12, 16$, and 28, with symmetry point groups T_h , T_d , and T ; (9) barrels were a common motif within the predicted GM structures; (10) bulklike wurtzite, or multilayered clusters, as well as the simple cuboid and related rock salt configurations were not found to be thermodynamically stable in the size range considered.

The size of the clusters found depends on n and the motif adopted: 2D rings ($n = 2–7$) have a diameter less than 0.8 nm, while spheroid bubbles (up to $n = 32$) are less than 1.2 nm, although tubular structures can have a longer length. In subsequent studies we shall investigate and predict the electronic properties of the structures reported. Furthermore, we will extend our search for the GM and low energy metastable structures to larger sizes, where care is required during the search so that both single and multilayered bubbles are fully explored.

Acknowledgment. We are grateful to EPSRC (Portfolio Grant EP/D504872) and KFUPM for funding and the British Council in Saudi Arabia for financing a visiting fellowship. Accelrys is thanked for the provision of the Materials Studio visualizer, Julian D. Gale for the GULP code, and Lee Whitmore for the ZnO potential parameters. We also thank Said Hamad, François-Xavier Coudert, and Emilio Artacho for useful discussions.

References and Notes

- Özgür, Ü.; Alivov, Ya. I.; Liu, C.; Teke, A.; Reschikov, M. A.; Doğan S.; Avrutin, V.; Cho, S.-J.; Markoç, H. *J. Appl. Phys.* **2005**, 98, 041301.
- Pearton, S. J.; Norton, D. P.; Ip, K.; Heo, Y. W.; Steiner, T. *Prog. Mater. Sci.* **2005**, 50, 293.
- Look, D. C.; Clafin, B. *Phys. Status Solidi B* **2004**, 241, 624.
- Wood, A.; Giersig, M.; Hilgendorff, M.; Vilas-Campos, A.; Liz-Marzán, L. M.; Mulvaney, P. *Aust. J. Chem.* **2003**, 56, 1051.
- Kumpf, C. *Appl. Phys. A: Mater. Sci. Process.* **2006**, 85, 337.
- Brus, L. *J. Phys. Chem.* **1986**, 90, 2555.

- (7) Pesilka, N. S.; Stebe, K. J.; Searson, P. C. *J. Phys. Chem. B* **2003**, *107*, 10412.
- (8) Guo, L.; Yang, S.; Yang, C.; Yu, P.; Wang, J.; Ge, W.; Wong, G. K. L. *Appl. Phys. Lett.* **2000**, *76*, 2901.
- (9) Wu, L. Y. L.; Tok, A. I. Y.; Boey, F. Y. C.; Zeng, X. T.; Zhang, X. H. *IEEE Trans. Nanotechnol.* **2007**, *6*, 497.
- (10) Masuda, Y.; Yamagishi, M.; Seo, W. S.; Koumoto, K. *Cryst. Growth Design* **2008**, *8*, 1503.
- (11) Kurbanov, S. S.; Panin, G. N.; Kim, T. W.; Kang, T. W. *Opt. Commun.* **2007**, *276*, 127.
- (12) Gavartin, J. L.; Stoneham, A. M. *Phil. Trans. R. Soc. London, Ser. A* **2003**, *361*, 275.
- (13) Zhou, H.; Alves, H.; Hofmann, D. M.; Kriegseis, W.; Meyer, B. K. *Appl. Phys. Lett.* **2002**, *80*, 210.
- (14) Vostrikov, A. A.; Shishkin, A. V.; Timoshenko, N. I. *Russ. Chem. Bull., Int. Ed.* **2006**, *55*, 2291.
- (15) Vostrikov, A. A.; Shishkin, A. V.; Timoshenko, N. I. *Tech. Phys. Lett.* **2007**, *33*, 30.
- (16) Polarz, S.; Roy, A.; Merz, M.; Halm, S.; Schröder, D.; Schneider, L.; Bacher, G.; Kruis, F. E.; Driess, M. *SMALL* **2005**, *1*, 540.
- (17) Hartlieb, K. J.; Raston, C. L.; Saunders, M. *Chem. Mater.* **2007**, *19*, 5453.
- (18) Cannavò, D.; Knopp, G.; Radi, P.; Beaud, P.; Tulej, M.; Bodek, P.; Gerber, T.; Wokaun, A. *J. Mol. Struct.* **2006**, *782*, 67.
- (19) Burnin, A.; BelBruno, J. *J. Chem. Phys. Lett.* **2002**, *362*, 341.
- (20) Bulgakov, A. V.; Ozerov, I.; Marine, W. <http://arXiv.org/abs/physics/0311117>, 2003.
- (21) Kukreja, L. M.; Rohlfing, A.; Misra, P.; Hillenkamp, F.; Dreisewerd, K. *Appl. Phys. A: Mater. Sci. Process.* **2004**, *78*, 641.
- (22) Dmitruk, A.; Dmitruk, I.; Belosludov, R.; Kasuya, A.; Kawazoe, Y. Small ZnO clusters: laser ablation production and time-of-flight mass spectroscopic study, Abstract of EMRS Meeting, Symposium G, Strasburg, 2008.
- (23) Ozerov, I.; Nelson, D.; Bulgakov, A. V.; Marine, W.; Sentis, M. *Appl. Surf. Sci.* **2003**, *212*–213, 349.
- (24) Ozerov, I.; Bulgakov, A.; Nelson, D.; Castell, R.; Sentis, M.; Marine, W. *J. Phys. IV* **2003**, *108*, 37.
- (25) Ozerov, I.; Bulgakov, A.; Nelson, D.; Castell, R.; Marine, W. *Appl. Surf. Sci.* **2005**, *247*, 1.
- (26) Said, A.; Sajti, L.; Giorgio, S.; Marine, W. *J. Phys.: Conference Series* **2007**, *59*, 259.
- (27) Acquaviva, S.; D'Anna, E.; De Giorgi, M. L. *J. Appl. Phys.* **2007**, *102*, 073109.
- (28) Antony, J.; Chen, X. B.; Morrison, J.; Bergman, L.; Qiang, Y.; McCready, D. E.; Engelhard, M. H. *Appl. Phys. Lett.* **2005**, *87*, 241917.
- (29) Wark, M.; Kessler, H.; Schulz-Ekloff, G. *Microporous Materials* **1997**, *8*, 241.
- (30) Khouchaf, L.; Tuilier, M.-H.; Wark, M.; Soulard, M.; Kessler, H. *Microporous Mesoporous Mater.* **1998**, *20*, 27.
- (31) Meneau, F.; Sankar, G.; Morgante, N.; Cristol, S.; Catlow, C. R. A.; Thomas, J. M.; Greaves, G. N. *Nucl. Instr. Meth. B* **2003**, *199*, 499.
- (32) Chen, J.; Feng, Z.; Ying, P.; Li, C. *J. Phys. Chem. B* **2004**, *108*, 12669.
- (33) Bouvy, C.; Marine, W.; Sporken, R.; Su, B. L. *Colloids Surfaces A: Physicochem. Eng. Aspects* **2007**, *300*, 145.
- (34) Readman, J.; Gameson, I.; Hriljac, J. A.; Edwards, P. E.; Anderson, P. A. *Chem. Commun.* **2000**, 595.
- (35) Muntele, I.; Muntele, C.; Thevenard, P.; Ila, D. *Surf. Coating Technol.* **2007**, *201*, 8557.
- (36) Wu, S.; Yuan, N.; Xu, H.; Wang, X.; Schelly, Z. A. *Nanotechnology* **2006**, *17*, 4713.
- (37) Matxain, J. M.; Mercero, J. M.; Fowler, J. E.; Ugalde, J. M. *J. Am. Chem. Soc.* **2003**, *125*, 9494.
- (38) Behrman, E. C.; Foehrweiser, R. K.; Myers, J. R.; French, B. R.; Zandler, M. E. *Phys. Rev. A* **1994**, *49*, R1543.
- (39) Zandler, M. E.; Behrman, E. C.; Arrasmith, M. B.; Myers, J. R.; Smith, T. V. *J. Mol. Struct.* **1996**, *362*, 215.
- (40) Matxain, J. M.; Fowler, J. E.; Ugalde, J. M. *Phys. Rev. A* **2000**, *62*, 053201.
- (41) Jain, A.; Kumar, V.; Kawazoe, Y. *Comput. Mater. Sci.* **2006**, *36*, 258.
- (42) Reber, A. C.; Khanna, S. N.; Hunjan, J. S.; Beltran, M. R. *Chem. Phys. Lett.* **2006**, *428*, 376.
- (43) Reber, A. C.; Khanna, S. N.; Hunjan, J. S.; Beltran, M. R. *Eur. Phys. J. D* **2007**, *43*, 221.
- (44) Zhao, M.; Xia, Y.; Tan, Z.; Liu, X.; Mei, L. *Phys. Lett. A* **2007**, *372*, 39.
- (45) Li, C.; Guo, W.; Kong, Y.; Gao, H. *Appl. Phys. Lett.* **2007**, *90*, 223102.
- (46) Zhu, Z.; Chutia, A.; Sahnoun, R.; Koyama, M.; Tsuboi, H.; Hatakeyama, N.; Endou, A.; Takaba, H.; Kubo, M.; Del Caprio, C. A.; Miyamoto, A. *Jpn. J. Appl. Phys.* **2008**, *47*, 2008.
- (47) Joswig, J.-O.; Roy, S.; Sarkar, P.; Springborg, M. *Chem. Phys. Lett.* **2002**, *365*, 75.
- (48) Wang, B.; Nagas, S.; Zhao, J.; Wang, G. *J. Phys. Chem. C* **2007**, *111*, 4956.
- (49) Wang, B.; Wang, X.; Chen, G.; Nagase, S.; Zhao, J. *J. Chem. Phys.* **2008**, *128*, 144710.
- (50) Lim, H. M.; Han, C. S. *Bull. Korean Chem. Soc.* **1999**, *20*, 1.
- (51) Hartke, B. *Struct. Bonding* **2004**, *110*, 35.
- (52) Roberts, C.; Johnston, R. L. *Phys. Chem. Chem. Phys.* **2001**, *3*, 5024.
- (53) Flikkema, E.; Bromley, S. T. *J. Phys. Chem. B* **2004**, *108*, 9638.
- (54) Hamad, S.; Catlow, C. R. A.; Woodley, S.; Lago, S.; Mejias, J. A. *J. Phys. Chem. B* **2005**, *109*, 15741.
- (55) Woodley, S. M. *Struct. Bonding* **2004**, *110*, 95.
- (56) Asmis, K. R.; Sauer, J. *Mass Spec. Rev.* **2007**, *26*, 542.
- (57) Whitmore, L.; Sokol, A. A.; Catlow, C. R. A. *Surf. Sci.* **2002**, *498*, 135.
- (58) Catlow, C. R. A.; French, S. A.; Sokol, A. A.; Al-Sunaidi, A. A.; Woodley, S. M. *J. Comput. Chem.* In press.
- (59) Gale, J. D. *J. Chem. Soc., Faraday Trans.* **1997**, *93*, 629.
- (60) Woodley, S. M.; Battle, P. D.; Gale, J. D.; Catlow, C. R. A. *Phys. Chem. Chem. Phys.* **1999**, *1*, 2535.
- (61) Woodley, S. M.; Sokol, A. A.; Catlow, C. R. A. *Z. Anorg. Allg. Chem.* **2004**, *630*, 2343.
- (62) Spanó, E.; Hamad, S.; Catlow, C. R. A. *J. Phys. Chem. B* **2003**, *107*, 10337.
- (63) Hamad, S.; Catlow, C. R. A.; Spanó, E.; Matxain, J. M.; Ugalde, J. M. *J. Phys. Chem. B* **2005**, *109*, 2703.
- (64) Woottton, A.; Harrowell, P. *J. Phys. Chem. B* **2004**, *108*, 8412.
- (65) Shevlin, S. A.; Guo, Z. X.; van Dam, H. J. J.; Sherwood, P.; Catlow, C. R. A.; Sokol, A. A.; Woodley, S. M. *Phys. Chem. Chem. Phys.* **2008**, *10*, 1944.
- (66) Miller, M.; Doye, J. P. K.; Wales, D. J. *J. Chem. Phys.* **1999**, *110*, 328.
- (67) Despa, F.; Wales, D. J.; Berry, R. S. *J. Chem. Phys.* **2005**, *122*, 024103.
- (68) Cox, G.; Berry, R. S.; Johnston, R. L. *J. Phys. Chem. A* **2006**, *110*, 11543.

JP805983G